Bulletin of the New Zealand Society for Earthquake Engineering, Vol. 52, No. 1, March 2019

IMPACTS OF SURFACE FAULT RUPTURE ON RESIDENTIAL STRUCTURES DURING THE 2016 M_W 7.8 KAIKŌURA EARTHQUAKE, NEW ZEALAND

Russ J. Van Dissen[1], Timothy Stahl[2], Andrew King[3], Jarg R. Pettinga[4], Clark Fenton[5], Timothy A. Little[6], Nicola J. Litchfield[7], Mark W. Stirling[8], Robert M. Langridge[9], Andrew Nicol[10], Jesse Kearse[11], David J. A. Barrell[12] and Pillar Villamor[13]

(Submitted *June 2018*; Reviewed *September 2018*; Accepted *October 2018*)

ABSTRACT

Areas that experience permanent ground deformation in earthquakes (e.g., surface fault rupture, slope failure, and/or liquefaction) typically sustain greater damage and loss compared to areas that experience strong ground shaking alone. The 2016 M_w 7.8 Kaikōura earthquake generated ≥220 km of surface fault rupture. The amount and style of surface rupture deformation varied considerably, ranging from centimetre-scale distributed folding to metre-scale discrete rupture. About a dozen buildings – mainly residential (or residential-type) structures comprising single-storey timber-framed houses, barns and wool sheds with lightweight roofing material – were directly impacted by surface fault rupture with the severity of damage correlating with both local discrete fault displacement and local strain. However, none of these buildings collapsed. This included a house built directly atop a discrete rupture that experienced ~10 m of lateral offset. The foundation and flooring system of this structure allowed decoupling of much of the ground deformation from the superstructure thus preventing collapse. Nevertheless, buildings directly impacted by surface faulting suffered greater damage than comparable structures immediately outside the zone of surface rupture deformation. From a life-safety standpoint, all these buildings performed satisfactorily and provide insight into construction styles that could be employed to facilitate non-collapse performance resulting from surface fault rupture and, in certain instances, even post-event functionality.

INTRODUCTION

The Kaikōura earthquake struck at two minutes past midnight on 14 November 2016. Its epicentre was located near the South Island township of Waiau (Figure 1) and, with a magnitude of M_w 7.8, it was the largest on-land earthquake to hit New Zealand in more than a century [1, 2]. The Kaikōura earthquake generated damaging levels of ground shaking throughout much of north Canterbury, eastern Marlborough and beyond [7, 8]. It triggered thousands of landslides [9, 10], and locally significant liquefaction [11-13]. The earthquake caused vertical deformation, primarily uplift, along more than 100 km of coastline between Cape Campbell and the Hundalee Fault south of Kaikōura [14] (Figure 1), and spawned a tsunami with up to ~7 m run-up height – the impacts of which were lessened by the fact that the earthquake occurred at low tide, and much of the potentially affected coastline had been uplifted [15].

In a global context, the Kaikōura earthquake was also one of the most complex earthquakes yet documented with about two-dozen major and minor faults rupturing the ground surface (Figure 1) [3, 16, 17]. Collectively, over 220 km of surface fault rupture was generated by the Kaikōura earthquake (Figure 1). This rupture directly impacted about a dozen residential (or residential-type) structures. In this paper, we document several examples of the impacts this surface fault rupture had on these buildings. We conclude with a brief discussion of the implications of these observations in relation to residential structures and the future mitigation of surface fault rupture hazard through land use planning and engineering design.

RESIDENTIAL STRUCTURES

About a dozen buildings, mostly single-storey timber-framed houses, barns and wool sheds, were directly impacted by surface fault rupture in the Kaikōura earthquake [17]. Below, we present eight informative case-study examples.

Bluff Cottage – Kekerengu Fault

Of the residential structures impacted by surface fault rupture during the Kaikōura earthquake, Bluff Cottage (Figures 1-3)

[1] *Corresponding Author, Senior Scientist, GNS Science, Lower Hutt, r.vandissen@gns.cri.nz (Fellow)*
[2] *Lecturer, University of Canterbury, Christchurch, timothy.stahl@canterbury.ac.nz*
[3] *Senior Scientist (retired), GNS Science, Lower Hutt (Life Member)*
[4] *Professor, University of Canterbury, Christchurch, jarg.pettinga@canterbury.ac.nz*
[5] *Senior Lecturer, University of Canterbury, Christchurch, clark.fenton@canterbury.ac.nz*
[6] *Professor, Victoria University of Wellington, Wellington, tim.little@vuw.ac.nz*
[7] *Senior Scientist, GNS Science, Lower Hutt, n.litchfield@gns.cri.nz*
[8] *Professor, University of Otago, Dunedin, mark.stirling@otago.ac.nz (Fellow)*
[9] *Senior Scientist, GNS Science, Lower Hutt, r.langridge@gns.cri.nz*
[10] *Professor, University of Canterbury, Christchurch, andy.nicol@canterbury.ac.nz*
[11] *MSc graduate, Victoria University of Wellington, Wellington, jesse@kearse.co.nz*
[12] *Senior Scientist, GNS Science, Dunedin, d.barrell@gns.cri.nz*
[13] *Senior Scientist, GNS Science, Lower Hutt, p.villamor@gns.cri.nz*

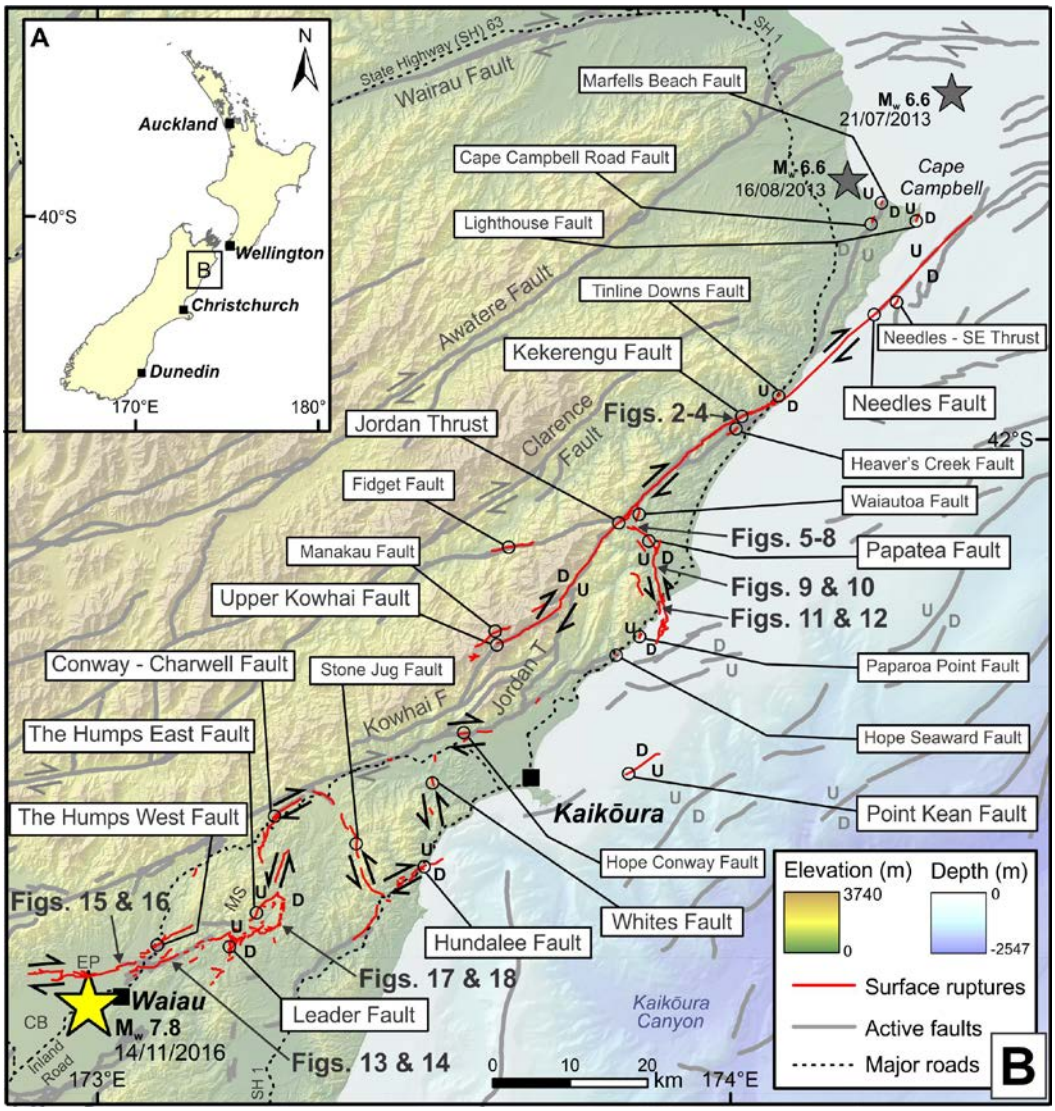

Figure 1: Kaikōura earthquake surface fault ruptures (red lines) from Litchfield et al. [3]. Also shown are the locations of Figures 2-18, the epicentre of the 2016 Kaikōura earthquake (large yellow star) from Nicol et al. [4], and the epicentres for the two 2013 Cook Strait earthquakes (small grey stars) from Holden et al. [5]. Abbreviations: CB = Culverden Basin, EP = Emu Plains, F = fault, MS = Mt. Stewart Range, T = thrust. A 1:250,000 scale digital version of 2016 surface ruptures is available for download at https://data.gns.cri.nz/af/ (choose Download Data – Kaikoura; Langridge et al. [6]).

deserves special mention because of its noteworthy life-safety (non-collapse) performance when subjected to extreme surface fault rupture deformation. Bluff Cottage – which has since been demolished – was a timber-framed single-storey residential structure (house) with a corrugated metal roof, and a combination of timber weather board and concrete brick cladding (Table 1). It had a roughly rectangular floor plan (area of ~90 m^2), a timber floor comprising a combination of particle board sheets and tongue and groove hardwood strips/planks, and a pre-cast concrete chimney and fireplace (with some steel-rod reinforcing) encased by concrete brick. It had a concrete perimeter foundation with shallow seated concrete piles. The timber floor joists were skew nailed to the timber wall plates which were in turn bolted to the perimeter foundation, and the timber floor bearers were attached to the piles via wire ties.

The age of construction of Bluff Cottage is composite, and not known in detail. The original hut that forms the core of the cottage was constructed prior to the late 1940s (the oldest set of aerial photographs for this part of the country date from 1947 and show that the hut was already in existence). Later, in the late 1970s / early 1980s a kitchen and sitting room were added along with the concrete perimeter foundation. Bluff Cottage was sited on a relatively thin layer (<1-2 m) of Holocene loosely packed gravel-dominated Kekerengu River alluvium overlying weak, fault-damaged, bedrock (Table 2).

Approximately 10 m of discrete (i.e., concentrated – as opposed to distributed) horizontal and 1-2 m vertical surface fault rupture displacement extended through the foot-print of Bluff Cottage on the Kekerengu Fault (Figure 3) [18]. Offset fence lines within ~450 m either side of the cottage also document lateral displacements of ~10-11 m and narrow fault deformation zone widths (Figures 2 & 4). The foundation of Bluff Cottage was cut in half and displaced by fault rupture. The superstructure of the house was low mass, flexible, regular in shape, timber floored and relatively weakly attached to the foundation. These properties allowed the superstructure to detach from the mainly laterally displacing foundation, and to isolate it from the extreme ground deformation taking place beneath. The house suffered severe structural damage, but it did not collapse. From a life-safety perspective, and considering the large displacement and small fault zone width at this site (i.e., metre-scale strike-slip displacements and shear strains in the order of 10^0; Table 2), this house performed admirably.

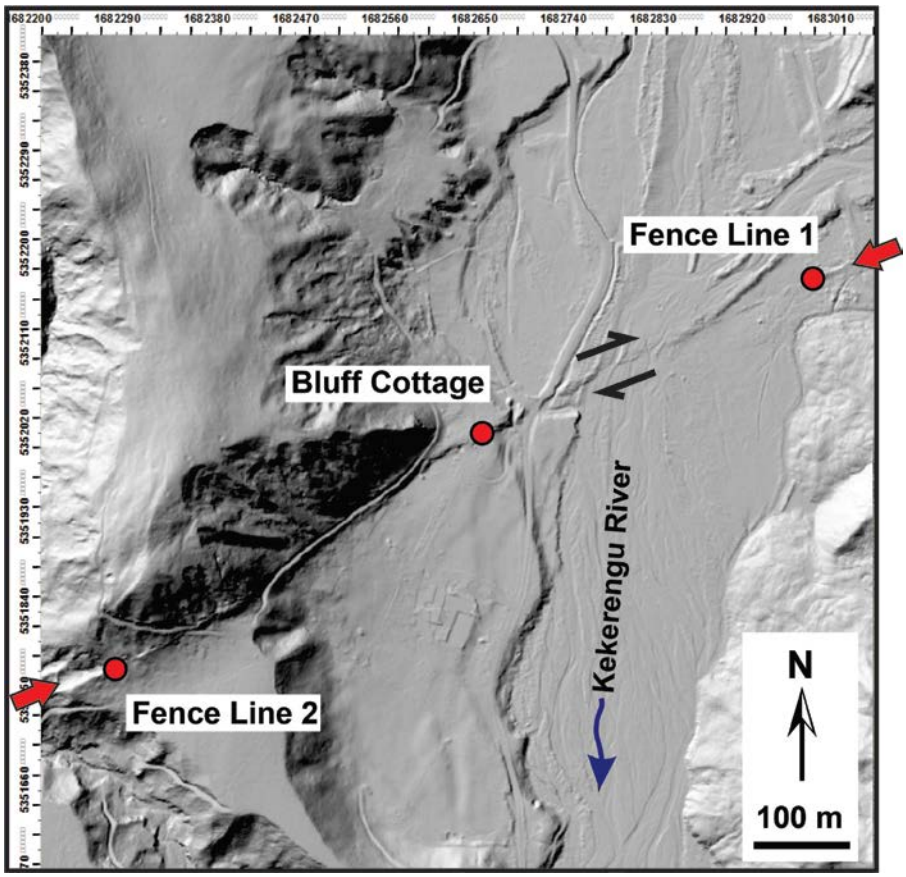

Figure 2: 2016 post-earthquake LiDAR hill shade DEM illuminated from the NW showing location of surface rupture trace of the Kekerengu Fault (red arrows), Bluff Cottage (Figure 3), the two offset fence lines depicted in Figure 4, and the sense of strike-slip on the Kekerengu Fault (black arrows). Though the size of Bluff Cottage portrayed in this figure is significantly exaggerated, its orientation is accurate. Coordinates are New Zealand Transvers Mercator 2000.

On the night of the earthquake, the occupant of Bluff Cottage had just gone to bed when the shaking started. Initially he braced himself in a doorway, but as the shaking intensified he rushed out of the house, jumped off the veranda, and ran into the open paddock/lawn immediately to the SE of the cottage (Figure 3A). It was a full moon and he reports seeing trees violently swaying and the power lines sparking as they were torn from the cottage. The noise, he says, was incredible. By his reckoning about a minute after the shaking started, the ground ruptured through the cottage. He reports that while watching the cottage and struggling to stand, his right leg went up and his left leg went down. Apparently, he was literally standing astride the Kekerengu Fault when surface rupture propagated through this site.

Harkaway Villa – Papatea Fault

Harkaway Villa is a timber-framed single-storey house with timber weather board cladding and a corrugated metal roof on framed rafters with internal load-bearing walls (Figures 1, 5 & 6; Table 1). It has a roughly square floor plan (area of ~130 m^2), timber strip (plank) flooring, and a timber pile foundation (~60 cm above ground) with joists attached to piles via wire ties and skew nails.

The age of construction of Harkaway Villa is composite. It was built around 1910. About a hundred years later, in 2009, it was moved onto the site (in three pieces) and, at this time, significant renovations were undertaken. The villa is sited on several metres of late Holocene fan alluvium (comprising interbedded silt, sand and loosely packed gravel) which, in turn, likely overlies gravel-dominated Clarence River alluvium.

Harkaway Villa is located within the surface rupture deformation zone of the Papatea Fault which, at this site, is ~90 m wide, comprising both discrete fault rupture and distributed deformation, and accommodating ~5 m of vertical deformation (reverse, SW side up) and a comparable (or lesser) amount of left-lateral horizontal slip (Figures 5-7) [19]. The villa is situated ~200 m west from the true-right bank of the Clarence River on the hanging-wall side (SW side) of the Papatea Fault in the hinge zone between the higher vertical displacement gradient fold/fault scarp to the NE and the lower vertical displacement gradient “back limb” to the SW (Figure 7). The ground encompassed by the foot-print of the structure experienced decimetre-scale folding, horizontal sinistral flexure (i.e., fault drag), and up to ~80 cm of distributed N-S oriented extension (Figures 6 & 7). The villa was also tilted ~5˚ in a down to the NE sense. Fortunately, the superstructure of the house is low mass, flexible, regular in shape, timber floored and relatively weakly attached to the pile foundation, all of which allowed the superstructure to detach from the foundation thus isolating much of the ground extension from the superstructure. Despite this house suffering damage significant enough to be “red tagged”, it - from a life-safety perspective - performed commendably. It experienced very strong ground shaking, local decimetre-scale surface fault rupture deformation and is located within the hinge zone of a reverse fault scarp that has been classified in other earthquakes as a zone of ‘severe building damage’ [20], yet the villa did not collapse. And, not only did the villa not collapse, it appears that it could potentially be re-piled and re-levelled, suggesting the possibility of post-event reinstatement (as opposed to demolition and reconstruction).

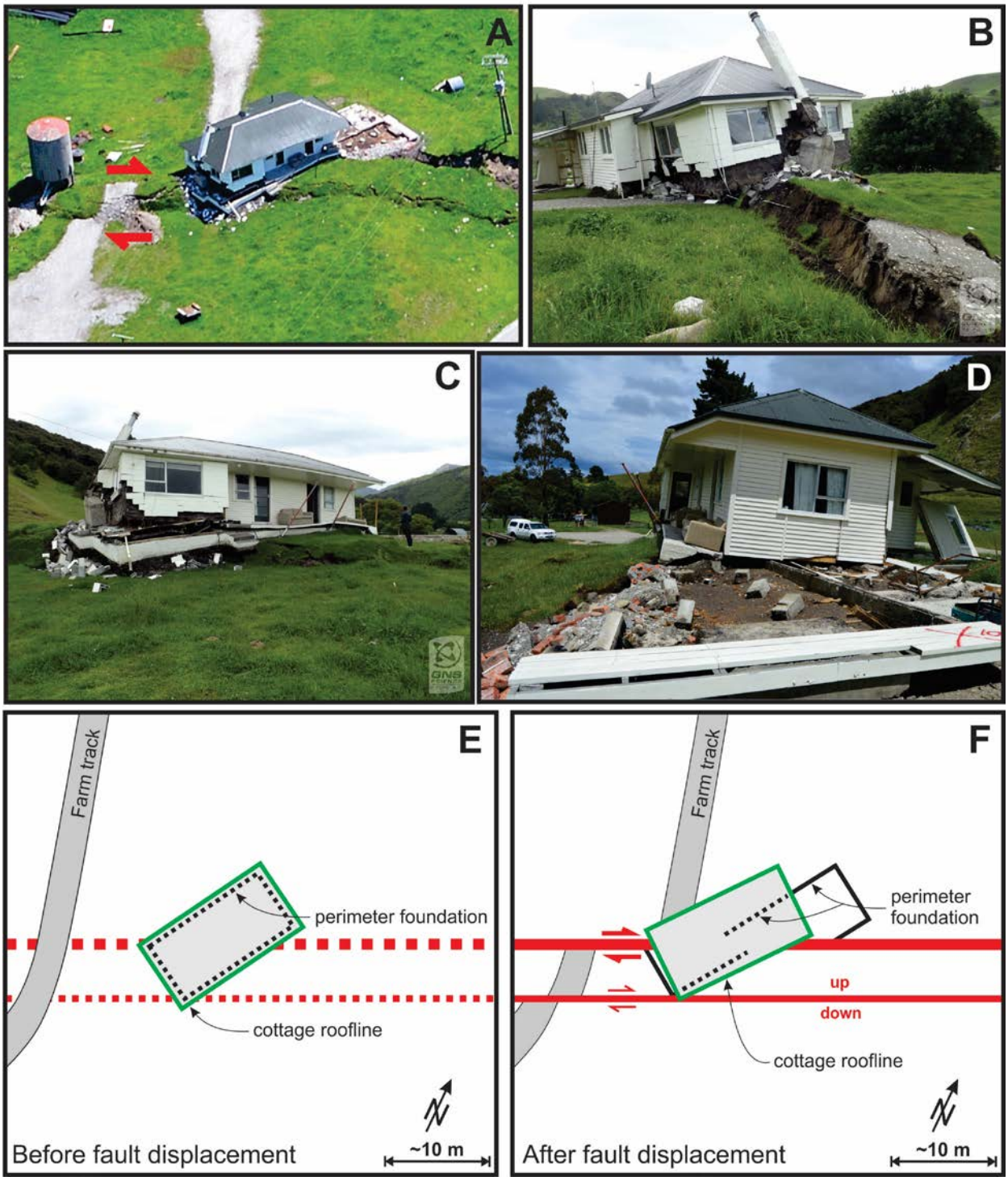

Figure 3: Bluff Cottage and Kekerengu Fault surface rupture; see Figure 1 for location (Lat: -41.9796, Long: 173.9976). (A) Oblique aerial view looking northwest. Red arrows show the sense of slip of the Kekerengu Fault that generated ~10 m of right-lateral surface rupture displacement at this locality. Photo by Dougal Townsend taken in November 2016. (B) View of Bluff Cottage looking northeast along the strike of the surface rupture of the Kekerengu Fault. Right-laterally offset farm track to left of cottage in Figure 3A is the same farm track visible in lower right and middle left of Figure 3B. Photo by Nicola Litchfield taken in November 2016. (C) View looking northwest. Photo by Nicola Litchfield taken in November 2016. (D) View looking southwest. Note that the concrete perimeter foundation and piles that were once under the cottage have now been torn from the superstructure of the cottage and laterally displaced towards the viewer relative to the cottage. Photo by Robert Zinke taken in November 2016. (E) Schematic map of Bluff Cottage and farm track prior to surface rupture of the Kekerengu Fault. (F) Schematic map of Bluff Cottage and farm track after fault displacement.

Table 1: Summary of building details.

Name of Building	Type of Structure	Number of Storeys	Framing	Cladding	Foundation	Roofing	Floor area (m^2)	Age of Construction	Figures in Text
Bluff Cottage	Residential	Single	Timber	Timber weather board & concrete brick	Concrete perimeter & concrete piles	Corrugated metal	~90	Pre late 1940s with additions in late 1970s / early 1980s	2 & 3
Harkaway Villa	Residential	Single	Timber	Timber weather board	Timber piles	Corrugated metal	~130	~1910 with alterations in 2009	5 & 6
Grey House	Residential	Single	Timber	Timber weather board	Concrete slab	Corrugated metal	~140	Pre early 1930s with alterations in 2004	5 & 8
Middle Hill Cottage	Residential	Single	Timber	Timber weather board	Timber piles	Corrugated metal	~75	Mid 1900s	9
Paradise Cottage	Residential	Single	Timber	Corrugated metal	Timber piles	Corrugated metal	~85	Pre early 1960s	12
Glenbourne Woolshed	Woolshed	Single	Timber	Corrugated metal	Concrete piles	Corrugated metal	~300	1980	13
Hillview Cottage	Residential	Single	Timber	Fibrolite	Concrete slab	Corrugated metal	~50	Pre early 1950s	15
Mendip Deer Shed	Deer shed	Single	Steel	Corrugated metal	light steel columns with concrete footings	Corrugated metal	~235	2004	17

Table 2: Summary of site conditions and surface fault rupture deformation.

Name of building	Site Conditions	Fault Name	Predominant Sense of Fault Displacement	Subordinate Sense of Fault Displacement	Amount of Discrete Fault Displacement Through Building Footprint	Shear Strain Across Building Footprint	Figures in Text
Bluff Cottage	Thin gravel over weak bedrock	Kekerengu	Dextral	Reverse	Metre-scale	10^{0}	2 - 4
Harkaway Villa	Interbedded silt, sand & gravel	Papatea	Reverse	Sinistral	Centimetre- to decimetre-scale	$10^{-2} – 10^{-1}$	6 & 7
Grey House	Interbedded silt, sand & gravel	Papatea	Reverse	Sinistral	Centimetre-scale	10^{-2}	8
Middle Hill Cottage	Gravel	Papatea	Reverse	Sinistral	Decimetre-scale	$10^{-2} – 10^{-1}$	9 & 10
Paradise Cottage	Gravel	Papatea	Reverse	Sinistral	Decimetre- to metre-scale	10^{-1}	11 & 12
Glenbourne Woolshed	Gravel over bedrock	The Humps	Dextral	Vertical	Decimetre-scale	10^{-2}	13 & 14
Hillview Cottage	Silt and gravel	The Humps	Dextral	Vertical	Decimetre-scale	10^{-2}	15 & 16
Mendip Deer Shed	Thin gravel over bedrock	Leader	Reverse	Horizontal	Centimetre- to decimetre-scale	$10^{-2} – 10^{-1}$	17 & 18

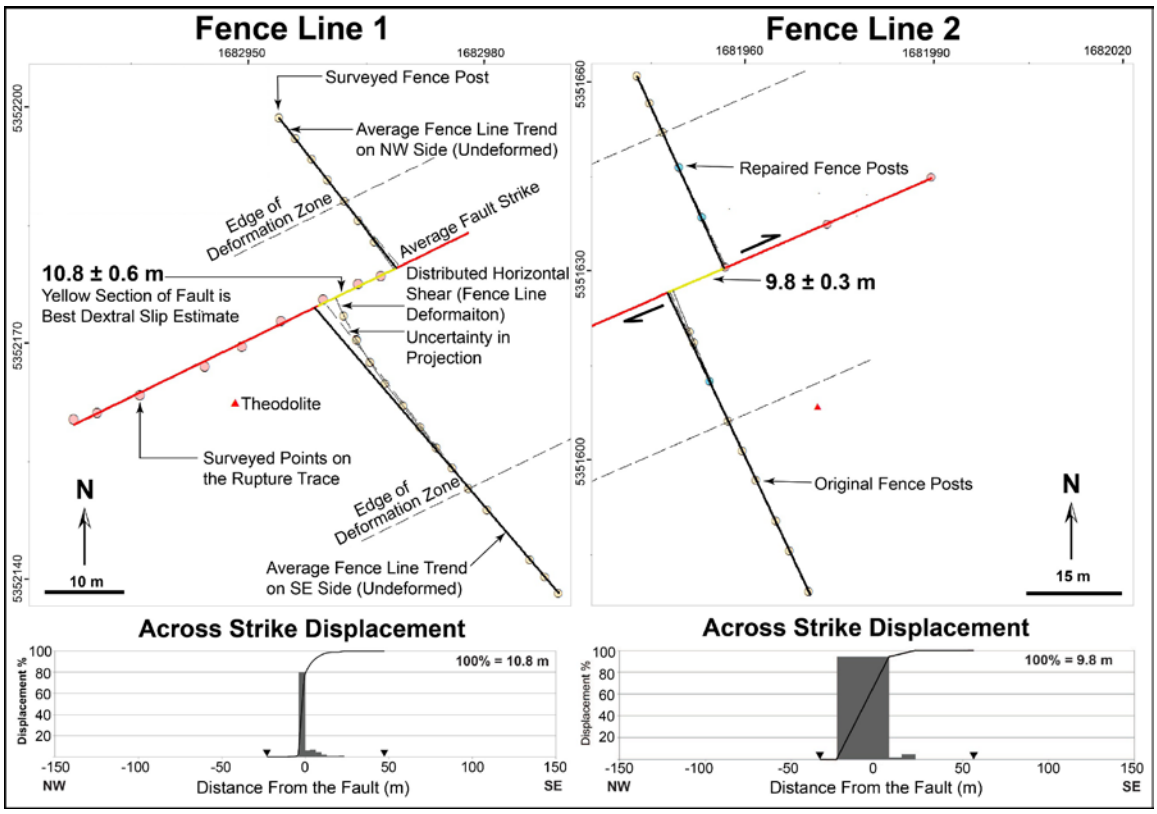

Figure 4: Examples of fence line displacements along the Kekerengu Fault near Bluff Cottage documenting both the amount of right-lateral displacement, and how that displacement is distributed as a function of distance perpendicular to fault strike (see Kearse et al. [18] for more detail). See Figure 2 for locations. Coordinates are New Zealand Transvers Mercator 2000.

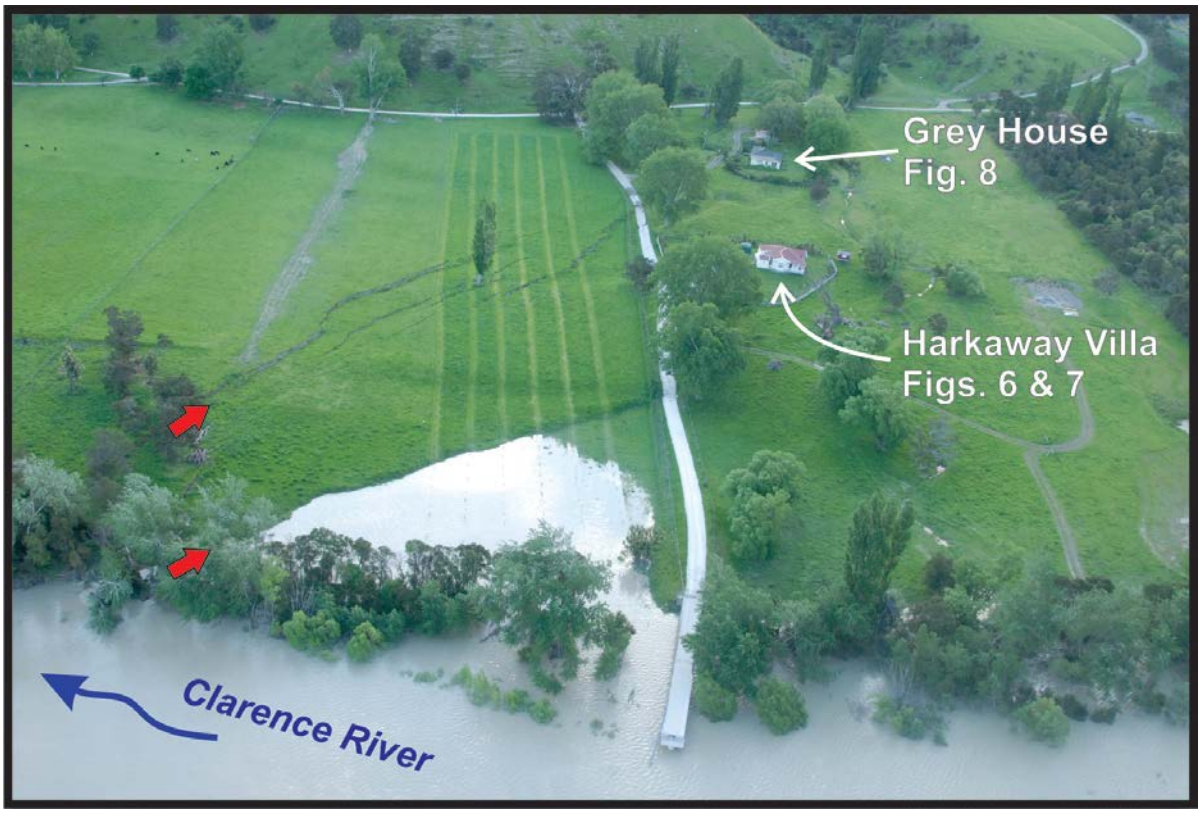

Figure 5: Harkaway Villa (Lat: -42.1105, Long: 173.8384), Grey House (Lat: -42.1105, Long: 173.8372, and the Papatea Fault surface rupture; see Figure 1 for location. Oblique aerial view looking west with red arrows denoting position of prominent discrete ruptures in the surface rupture deformation zone of the Papatea Fault. Photo by Will Ries taken in November 2016.

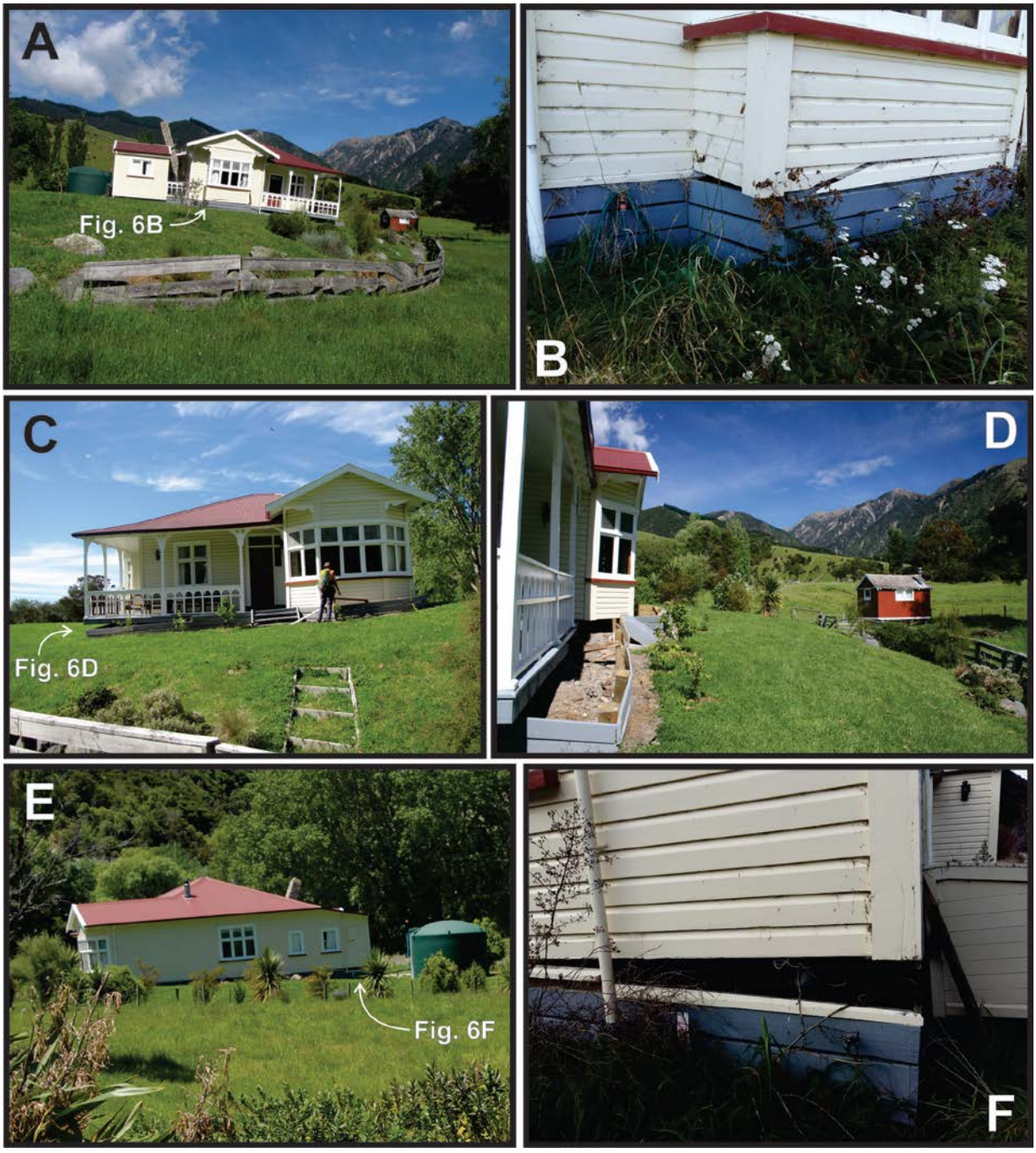

Figure 6: Harkaway Villa and Papatea Fault surface rupture. (A) View looking west showing northeastward tilt of the villa on the upthrown (hanging-wall) side of the Papatea Fault. Photo by Julie Rowland taken in November 2016. (B) View looking northwest showing detail of damage to the east-side of the villa. Photo by Julian Garcia-Mayordomo taken about 18 months after the 2016 Kaikōura earthquake. (C) View looking south of the north-side of the villa. Photo by Rob Langridge taken in November 2016. (D) View looking west of the north-side of the villa showing offset of the foundation piles from the superstructure. Photo by Julie Rowland taken in November 2016. (E) View looking east of the west-side of Harkaway Villa. Photo by Rob Langridge taken in November 2016. (F) View looking east showing detail of damage to the west-side of the villa. Photo by Julian Garcia-Mayordomo taken in May 2018.

As stated above, and illustrated in Figure 7, Harkaway Villa is located in the transition zone between the higher strain fold/fault scarp to the NE and the lower strain "back limb" to the SW. Utilising a combination of field observations, a differential Light Detecting and Ranging (LiDAR) digital elevation model (DEM; 2013 LiDAR subtracted from post-earthquake 2016 LiDAR) at the site (Figures 7B & 7C), and assuming simple shear, ground strains at the villa site can be approximated.

At the steepest portion of the fold/fault scarp region to the NE of the villa, dip-slip shear strains of ~0.2-0.4 can be derived based on ~1.5 m of elevation gain over 7 m of fault-perpendicular horizontal distance (Figure 7C), an estimated/observed fault dip of 45˚- 90˚ [19], and assuming simple shear. Strike-slip shear strains of ≤0.2 can be estimated based on an observed horizontal to vertical ratio of displacement of ≤1 [19], ~1.5 m of elevation gain over 7 m of fault-perpendicular horizontal distance, and assuming simple shear. Based on the above dip-slip and strike-slip shear strain considerations, net shear strains oriented parallel to the plane of the fault of ~0.2-0.4 (rounded to 10^{-1}) are approximated in the region of the fold/fault scarp.

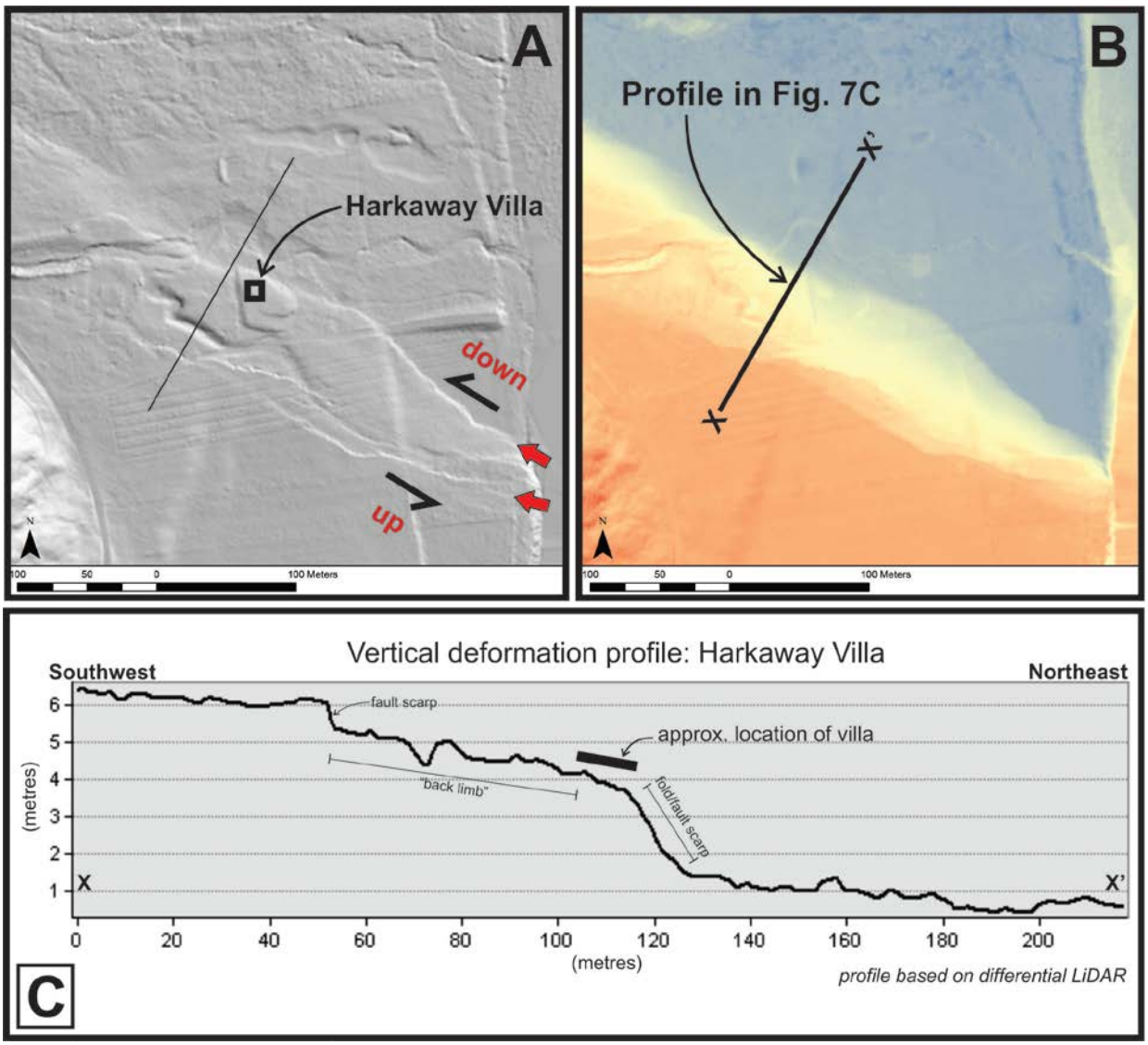

Figure 7: Harkaway Villa and Papatea Fault surface rupture. (A) 2016 post-earthquake LiDAR hill shade DEM with black square denoting villa's location, and red arrows showing location of prominent discrete ground surface ruptures. (B) Differential LiDAR DEM with blue colours denoting little vertical change and red colours denoting significant positive vertical change (see Figure 7C for more detail regarding scale). (C) Vertical deformation profile derived from the differential LiDAR DEM. Vertical exaggeration = 7.5.

In the "back limb" area, dip-slip shear strains of ~0.02-0.04 can be estimated based on ~1 m of elevation gain over 50 m of fault-perpendicular horizontal distance (Figure 7C), an estimated/observed fault dip of 45˚- 90˚ [19], and assuming simple shear. Strike-slip shear strains of ≤0.02 can be estimated based on an observed horizontal to vertical ratio of displacement of ≤1 [19], ~1 m of elevation gain over 50 m of fault-perpendicular horizontal distance, and assuming simple shear. In the "back limb" area, and based on the above dip-slip and strike-slip shear strain considerations, net shear strains oriented parallel to the fault plane of approximately 0.02-0.04 (rounded to 10^{-2}) are estimated.

Because Harkaway Villa is located between the fold/fault scarp and "back limb" regions, we estimate that the ground-surface beneath Harkaway Villa experienced fault-parallel net shear strains in the order of 10^{-2} – 10^{-1} (Table 2), comprising a combination of reverse dip-slip and left-lateral shear strain.

In addition, at the villa site, N-S oriented horizontal tensile strains of ~0.06 (rounded to 10^{-2}) are estimated based on the observation that the N-S extent of the villa's foundation piles was about 0.8 m greater than the ~13 m N-S length of the superstructure (Figure 6D).

Grey House – Papatea Fault

Grey House is a timber-framed single-storey residential structure with a corrugated metal roof and timber weather board cladding (Figures 5 & 8; Table 1). It has a concrete slab foundation that the owner reports as having been poured "double thick". It has a roughly square floor plan with an approximate area of 140 m^2.

Grey House was moved onto its present site in 1933. In 2004 the owner had the house placed on a concrete slab, and renovated the house "from top to bottom". The only original components of the house are the roof, and some weatherboards, windows and interior doors. The site conditions at Grey House are similar to those at Harkaway Villa (i.e., several metres of late Holocene fan alluvium that most likely overlie gravel-dominated Clarence River alluvium).

Grey House is located about 100 m west of Harkaway Villa within the surface rupture deformation zone of the Papatea

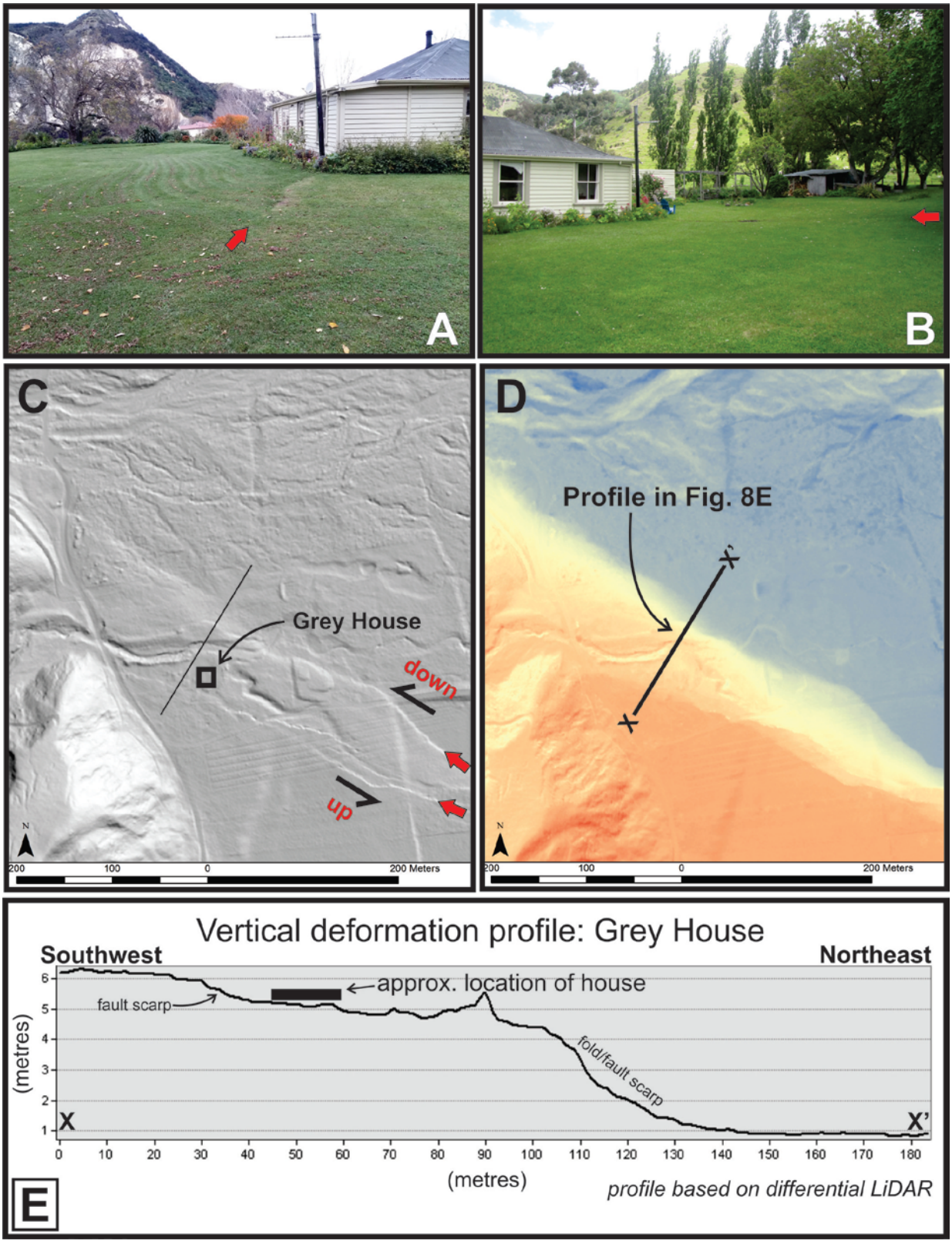

Figure 8: Grey House and Papatea Fault surface rupture. (A) View looking east-southeast with red arrow showing location of centimetre-scale discrete rupture that intersects northwest corner of the house. Harkaway Villa (Figures 5 & 6) is visible in the middle distance. Photo by Julia Garcia-Dayomo taken about 18 months after the 2016 Kaikōura earthquake. (B) View looking southwest. Red arrow denotes the location of centimetre-scale discrete rupture that intersects the northwest corner of the house. C) 2016 post-earthquake LiDAR hill shade DEM with the black square denoting the house's location, and red arrows showing the location of prominent discrete ground surface ruptures. (D) Differential LiDAR DEM with blue colours denoting little vertical change and red colours denoting significant positive vertical change (see Figure 8E for more detail regarding scale). (E) Vertical deformation profile derived from the differential LiDAR DEM. Vertical exaggeration = 6.4.

Fault. At this locality, the Papatea Fault accommodates approximately 6 m of vertical deformation (reverse, SW side up), and a comparable (or lesser) amount of left-lateral horizontal slip [19], and defines an ~100+ m wide surface fault rupture deformation zone comprising both discrete fault rupture and distributed deformation (Figure 8). The house is located on the hanging-wall side (SW side) of the Papatea Fault with metre-scale surface fault rupture passing within ~45 m NE of the house, metre- to decimetre-scale surface fault rupture passing within ~10 m SW of the house, and centimetre-scale surface fault rupture intersecting the foot-print of the house (Figures 8A & 8B). Nevertheless, the house came through the earthquake in good shape. It did not suffer significant structural damage, and following the earthquake it was adjudged suitable for habitation, and is currently occupied. In addition, the house is located within a portion of the surface rupture deformation zone that experienced minimal tilt, and this too no doubt facilitated post-event occupation.

Utilising a combination of field observations, a differential LiDAR DEM at the site (Figures 8D & 8E), and assuming simple shear, ground strains at the Grey House site can be approximated. At the location of the house, dip-slip shear strains of ~0.02-0.03 can be estimated based on ~0.5 m of elevation gain over 25 m of fault-perpendicular horizontal distance (Figure 8E), an estimated/observed fault dip of 45˚- 90˚ [19], and assuming simple shear. Strike-slip shear strains of ≤0.02 can be estimated based on an observed horizontal to vertical ratio of displacement of ≤1 [19], ~0.5 m of elevation gain over 25 m of fault-perpendicular horizontal distance, and assuming simple shear. Based on the above dip-slip and strike-slip shear strain considerations, net shear strains oriented parallel to the fault plane of ~0.03-0.04 (rounded to 10^{-2}; Table 2) are approximated at the Grey House site.

Middle Hill Cottage – Papatea Fault

Middle Hill cottage was a timber-framed single-storey residential structure with a corrugated metal roof, timber weather board cladding, and timber pile foundation (Figures 1, 9 & 10; Table 1). It had a roughly rectangular floor plan with an approximate area of 75 m^2.

Middle Hill Cottage was probably constructed in the mid 1900s (the oldest aerial photographs we have access to for this part of the country date from 1961 and show that the cottage was already in existence). It was sited on several metres of Holocene gravel-dominated fan alluvium that likely overlies gravel-dominated Clarence River alluvium.

Middle Hill Cottage was located within the surface rupture deformation zone of the Papatea Fault which, at this site, is ~100 m wide, comprising both discrete fault rupture and distributed deformation, and accommodating ~7.5 m of vertical deformation (reverse, W side up) and a comparable (or lesser) amount of left-lateral horizontal slip (Figures 9 & 10) [19]. The Cottage was located on the hanging-wall side of the Papatea Fault, close to the crest of the broad fold/fault scarp that is cut by extensional fissures (Figure 9C). The ground encompassed by the foot-print of the structure experienced decimetre-scale folding, horizontal sinistral flexure (i.e., fault drag), tilting, and distributed E-W oriented extension. As a result of the Kaikōura earthquake, this house suffered damage significant enough to be “red tagged”, and it has since been demolished. However, from a life-safety perspective, this house performed creditably - it experienced very strong ground shaking, tilting and decimetre-scale surface fault rupture deformation, but it did not collapse.

Utilising a combination of field observations and a differential LiDAR DEM at the site (Figures 10B & 10C), assuming simple shear, and adopting a fault dip of 45°-90° and a horizontal to vertical ratio of displacement of ≤1 [19], we estimate that the ground-surface beneath Middle Hill Cottage experienced fault-parallel net shear strains in the order of 10^{-2} – 10^{-1} (Table 2), comprising a combination of left-lateral and reverse dip-slip shear strain.

Paradise Cottage – Papatea Fault

Paradise Cottage is a timber-framed single-storey house with corrugated metal roof and cladding (Figures 11 & 12). It has a roughly square floor plan (area of ~85 m^2). Most of the structure is founded on timber piles, but the laundry room at the back of the cottage (W side of cottage) has a concrete slab foundation. About 13 m to the south of the cottage there is a timber framed and timber clad shed.

Paradise Cottage was constructed prior to the early 1960s (aerial photographs from 1961 show that the cottage was already in existence). Paradise Cottage is sited on several metres of Holocene gravel-dominated colluvium and alluvium, and beach sand and gravel, overlying moderately strong bedrock.

At the coast, where Paradise Cottage is located, the Papatea Fault comprises several main strands; the cottage is located across and immediately adjacent to the western most of these [19]. Here, the western strand of the Papatea Fault accommodates approximately 3.5 m of vertical deformation (E side up) (Figure 11D), a subordinate amount of left-lateral horizontal slip [19], and defines an 8-10 m wide surface fault rupture deformation zone primarily comprising discrete fault rupture. The cottage is located on the upthrown side of the fault, at the eastern edge of the surface rupture deformation zone, and has had its back-side ripped out by surface fault rupture. The nearby timber shed is located entirely within the fault scarp, and has been severely tiled and deformed. Neither the house nor the shed collapsed.

Employing a combination of field observations and a differential LiDAR DEM at the site (Figures 11C & 11D), assuming simple shear, and adopting a sub-vertical fault dip and a horizontal to vertical ratio of displacement of <1 [19], we estimate that the ground-surface beneath the shed and the SW corner of the cottage experienced fault-parallel net shear strains in the order of 10^{-1}.

Glenbourne Woolshed – The Humps Fault

The Glenbourne woolshed is a single storey, timber-framed structure with corrugated metal roof and cladding (Figures 13 & 14). It has a rectangular floor plan (area of ~300 m^2). The structure stands on concrete piles and has timber flooring overlying timber joists.

The Glenbourne Woolshed was constructed in 1980. It is sited on 2-4 m of late Pleistocene-Holocene loosely packed fluvial gravel above moderately strong bedrock.

Glenbourne Farm is located near the north-east margin of the Culverden Basin, where the low relief topography of the Emu Plains transitions into the steeper slopes of the Mt. Stewart Range (Figure 1). Here, surface rupture of The Humps Fault comprises 3-4 main traces mapped over a 3.5 km width perpendicular to fault strike (Figure 14) [4]. Net dextral displacement across these traces is a factor of 2 larger compared to the average dextral displacement on the western ~20 km of the fault [4]. Along the fault, vertical displacements are variably north- or south-side up. At the Glenbourne woolshed, surface rupture displacement was measured using RTK-GPS with the primary trace, located only ~5 m from the woolshed (Figures 13A, 13C & 14A), having ~1-2 m of dextral and ~1.2 m of north-side up vertical displacement. The woolshed is situated on the downthrown side of the primary discrete trace in a 10-

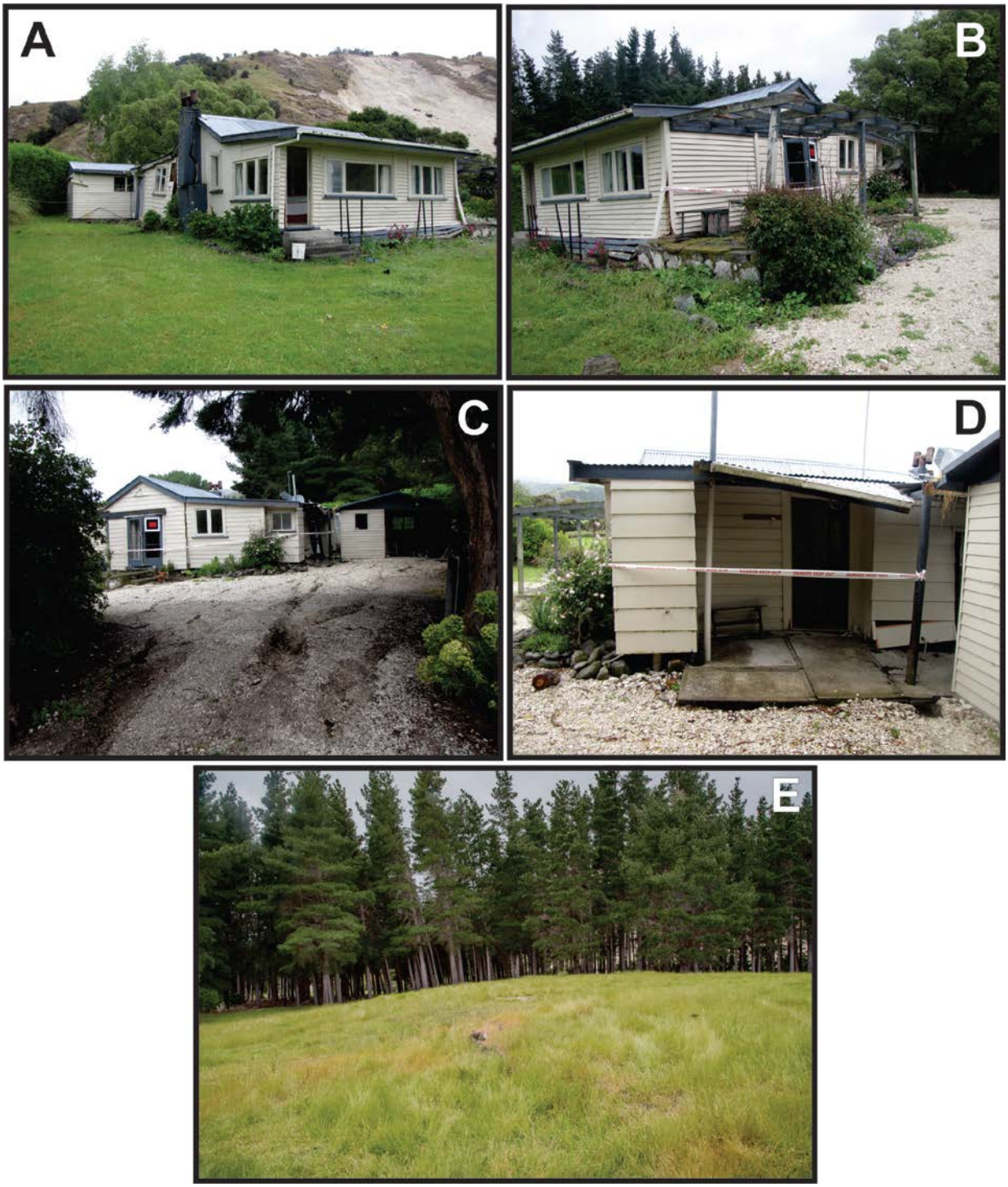

Figure 9: Middle Hill Cottage and Papatea Fault surface rupture; see Figure 1 for location (Lat: -42.1536, Long: 173.8667). (A) View looking west. Photo by Rob Langridge taken in December 2016. View looking south-southwest. Photo by Rob Langridge, December 2016. (C) View looking southeast along the strike of extensional fissures located in the crestal region of the primary fold/fault scarp that extend towards, and intersect, the cottage. Photo by Rob Langridge, December 2016. (D) View looking northeast. Photo by Rob Langridge, December 2016. (E) View from the cottage looking south-southeast along strike of the Papatea Fault's surface rupture deformation zone. Prior to the 2016 rupture of the Papatea Fault, the ground surface in this photograph was approximately flat and horizontal, and the trunks of the pine trees were all sub-vertical. Photo taken about a year after the earthquake by Stefano Pucci.

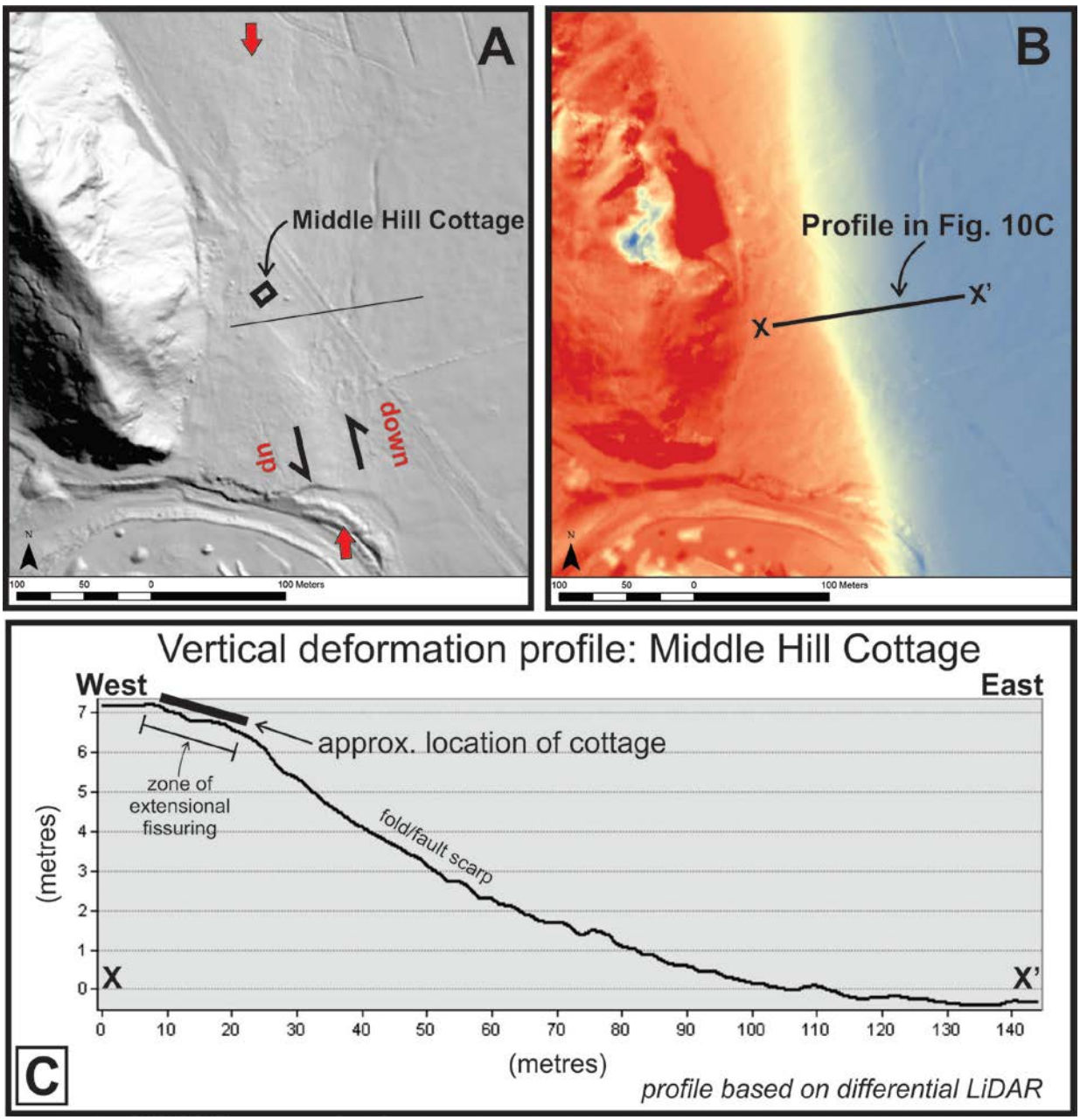

Figure 10: Middle Hill Cottage and Papatea Fault surface rupture. (A) 2016 post-earthquake LiDAR hill shade DEM with the black square denoting cottage's location, and red arrows showing the location the surface fault rupture scarp. (B) Differential LiDAR DEM with blue colours denoting little vertical change and red colours denoting significant positive vertical change (see Figure 10C for more detail regarding scale). (C) Vertical deformation profile derived from the differential LiDAR DEM. Vertical exaggeration = 6.1.

20 m wide zone of decimetre-scale ground subsidence that encompasses minor fracturing and small faults with vertical displacements of 1-10 cm (Figure 13A). This zone of ground subsidence extends from the stockyard adjacent to, and southwest of, the woolshed to the northeast for over 50 m. Fault rupture induced damage to the Glenbourne woolshed appears to be limited to rotation of some of the shallow-seated concrete piles (Figure 13B). The super structure itself is relatively undamaged and intact. We suspect that rotation of the piles isolated the super structure from the decimetre-scale fault rupture ground deformation underneath. It is pertinent to note that a similarly constructed, and piled, woolshed sited across the 2010 surface rupture of the Greendale Fault displayed similar performance with rotation of shallow-seated piles isolating, to a large extent, the super structure from the underlying fault rupture ground deformation [21].

At this location, and elsewhere along The Humps and Leader faults, we have access to pre- and post-earthquake photogrammetric point clouds. Iterative closest point (ICP) differencing of pre- and post-earthquake point clouds (e.g., Nissen et al. [22]) yields gridded values of displacements in the vertical, northing and easting directions at 50 m grid spacings. These gridded values were interpolated into three separate 10 m grid size rasters (one for each component/direction), and we construct fault-perpendicular transects on these rasters, crossing the structures, to estimate the fault-parallel net shear strains at the location of the structures that incorporate both horizontal and vertical displacements (Figure 14). Given the decametre-scale resolution of the ICP method, our shear strain estimations need to be augmented by field observations to take into account the location, and amount, of discrete displacements that would otherwise be smoothed by the ICP method. Nevertheless, the

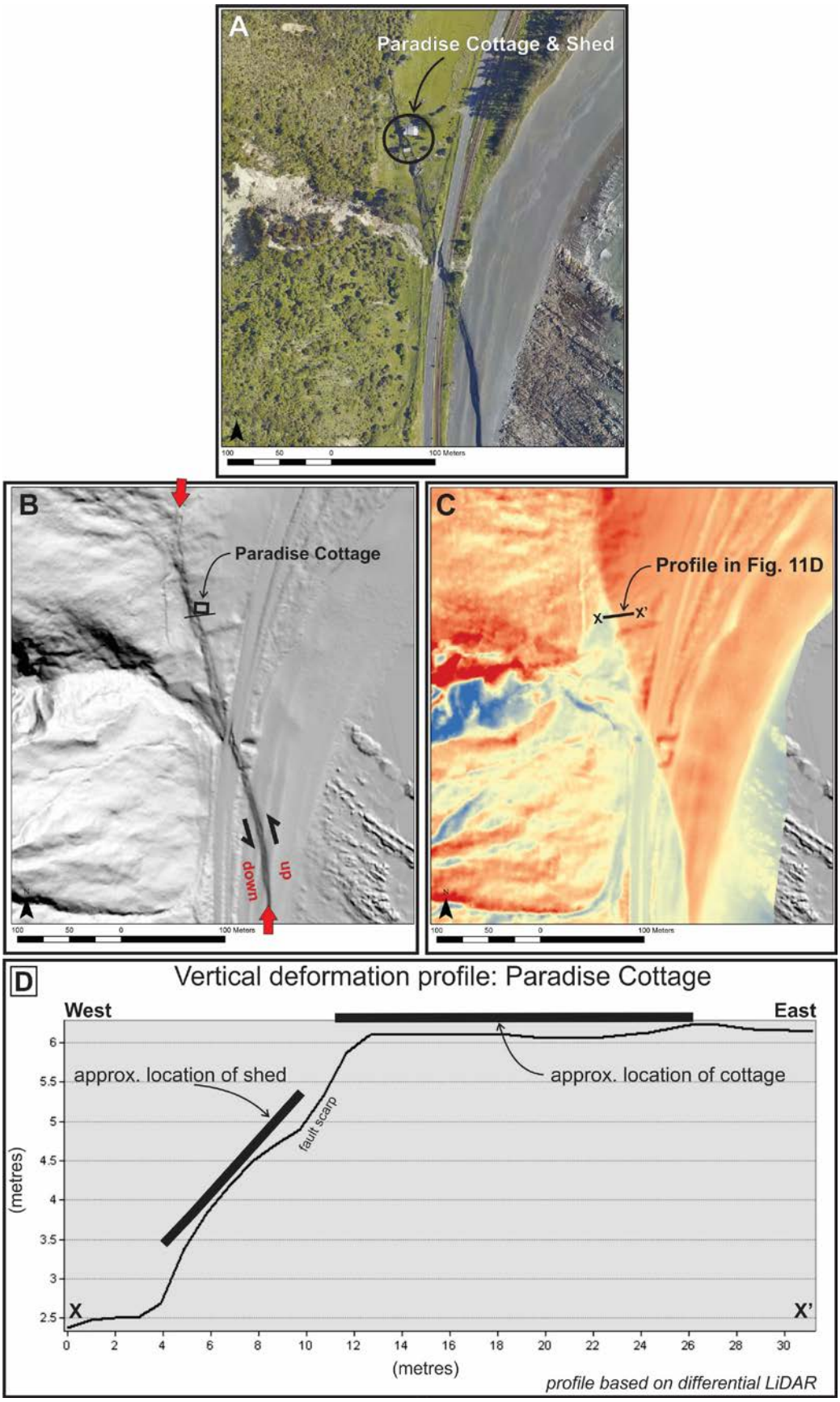

Figure 11: Paradise Cottage and Papatea Fault surface rupture; see Figure 1 for location (Lat: -42.2010, Long: 173.8753). (A) 2016 post-earthquake vertical aerial orthophotograph. Black circle denotes location of cottage and shed to the south. (B) 2016 post-earthquake LiDAR hill shade DEM showing location of cottage (black square) and prominent discrete ground surface ruptures (red arrows). (C) Differential LiDAR DEM with blue colours denoting little vertical change and red colours denoting significant positive vertical change (see Figure 11D for more detail regarding scale). (D) Vertical deformation profile derived from differential LiDAR DEM located half-way between the cottage and the shed. Vertical exaggeration = 3.3.

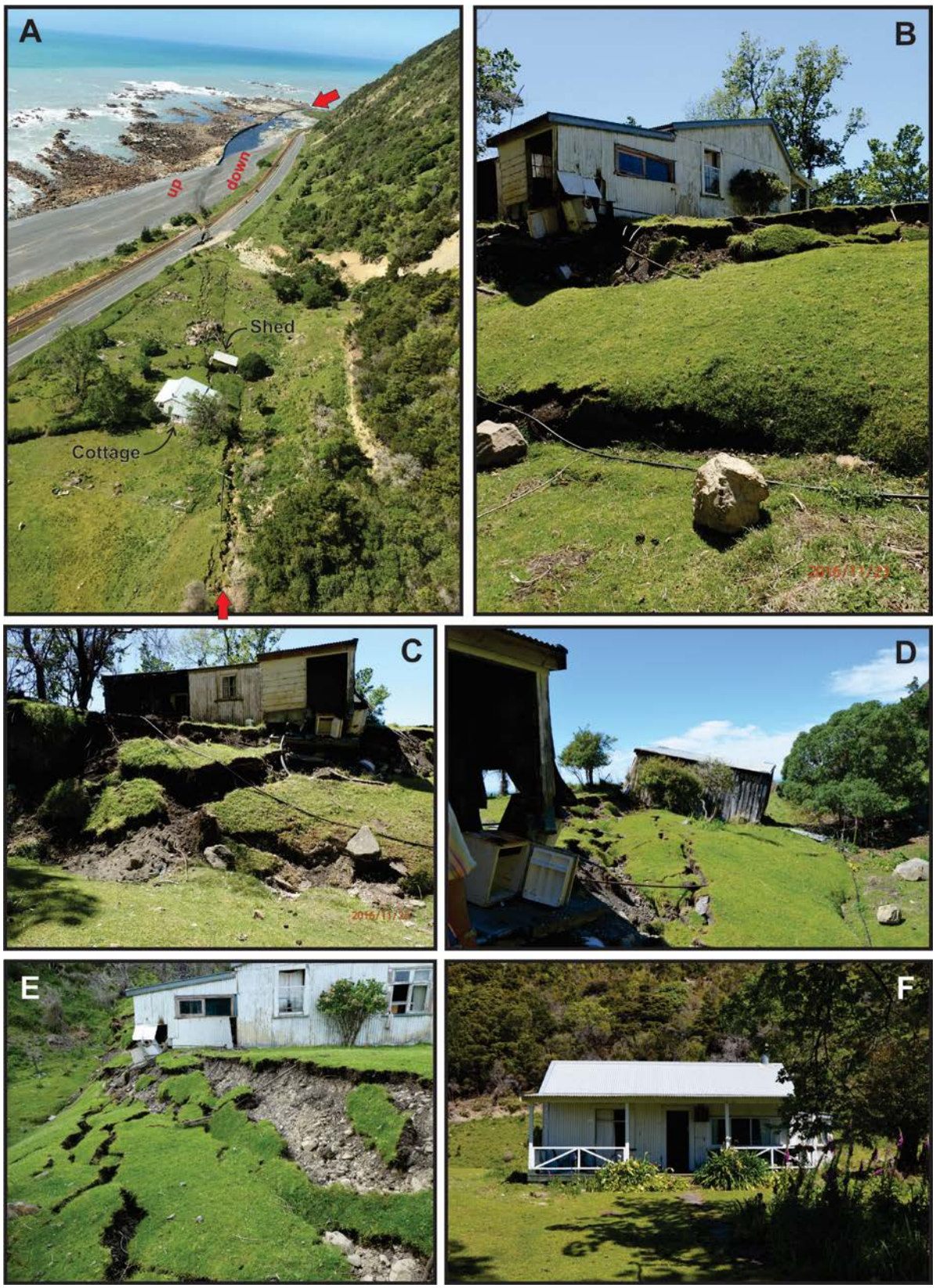

Figure 12: Paradise Cottage and Papatea Fault surface rupture; see Figure 1 for location. (A) Oblique aerial view looking south-southeast along the strike of the western strand of the Papatea Fault. Red arrows denote the position of prominent discrete rupture. Photo by Will Ries taken in November 2016. (B) View looking northeast. Photo by Alex Hatem taken in November 2016. (C) View looking east. Photo by Alex Hatem taken in November 2016. (D) View looking south-southeast towards the shed. Photo by Robert Zinke taken in November 2016. (E) View looking north-northwest along strike of the surface fault rupture. Photo by Tim Little taken in November 2016. (F) View looking east towards the front-side of the cottage. The front of the cottage appears to be little damaged and belies the havoc out back. Photo by Robert Zinke taken in November 2016.

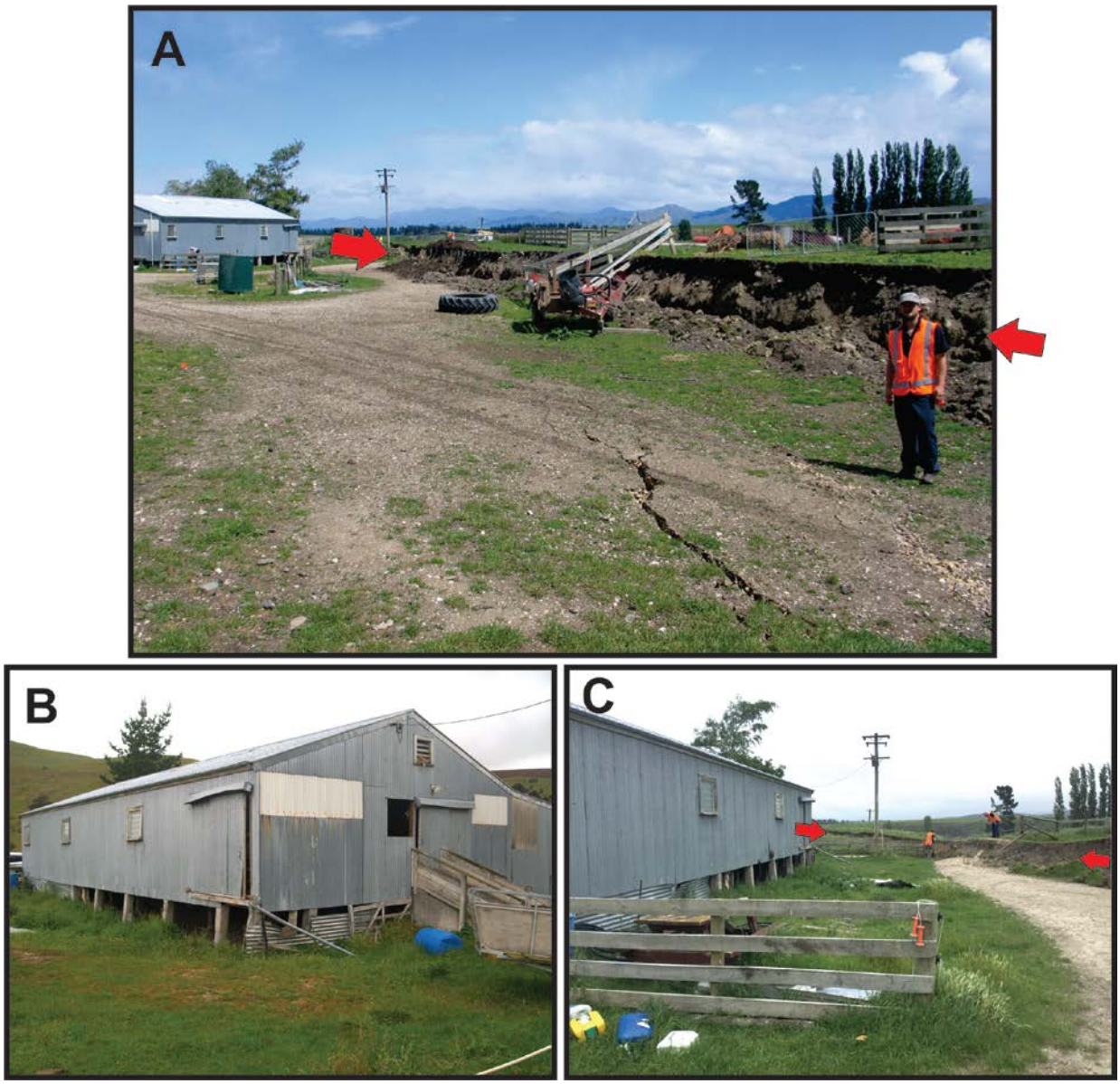

Figure 13: Glenbourne Woolshed and The Humps Fault surface rupture; see Figures 1 & 14 for location (Lat: -42.6152, Long: 173.1058). (A) View looking southwest along the fault rupture towards the woolshed. Note distributed centimetre-scale cracking in the foreground (in front of the high-vis geologist), adjacent to the main trace (red arrow, and behind the high-vis geologist). The distributed centimetre-scale cracking persists along strike for many tens of metres. Photo by Jarg Pettinga taken in November 2016. (B) View looking south at the woolshed (main fault scarp is behind the camera). Tilt and rotation of the shallow-seated concrete piles is the only recognisable damage. Photo by Clark Fenton taken in December 2016. (C) View looking southwest along the side of the woolshed and towards the main fault scarp at this site. Photo by Tim Stahl taken in November 2016.

ICP method provides the opportunity to document the amount and style of broad-scale net displacement across the surface rupture deformation zone, and distributed deformation within the deformation zone, that may otherwise not be readily apparent, or well characterised, by field measurements of discrete displacement alone. While the ICP method is used here to estimate 3D displacements that should be internally consistent across fault profiles, there is some uncertainty introduced in both gridding processes and this yields uncertainty regarding the exact amount and distribution of deformation along the profiles at the specific location of the structures. This, in turn, yields uncertainty in our strain estimations. However, we expect that this effect is small given the order of magnitude strain estimates reported in this paper, and acknowledging that field observations of discrete displacement are taken into account. Using this data, and assuming simple shear and a sub-vertical fault dip (80-90°) at the woolshed site, we estimate net shear strains of ~10-2.

Hillview Cottage – The Humps Fault

Hillview Cottage is a timber-framed, single-storey residential structure with a corrugated metal roof and Fibrolite cladding. It has a concrete slab foundation and has a rectangular floor plan with an area of ~50 m^2 (Figures 15 & 16).

Hillview Cottage was constructed prior to the early 1950s (aerial photographs from 1950 show that the cottage was already in existence). It is sited on >15 m of late Pleistocene loosely to tightly packed fan gravel and stiff loess.

Hillview Cottage is located on a zone of concentrated deformation in the central section of The Humps Fault. Just west of the cottage, there is a prominent, ~25 m-wide pull-apart

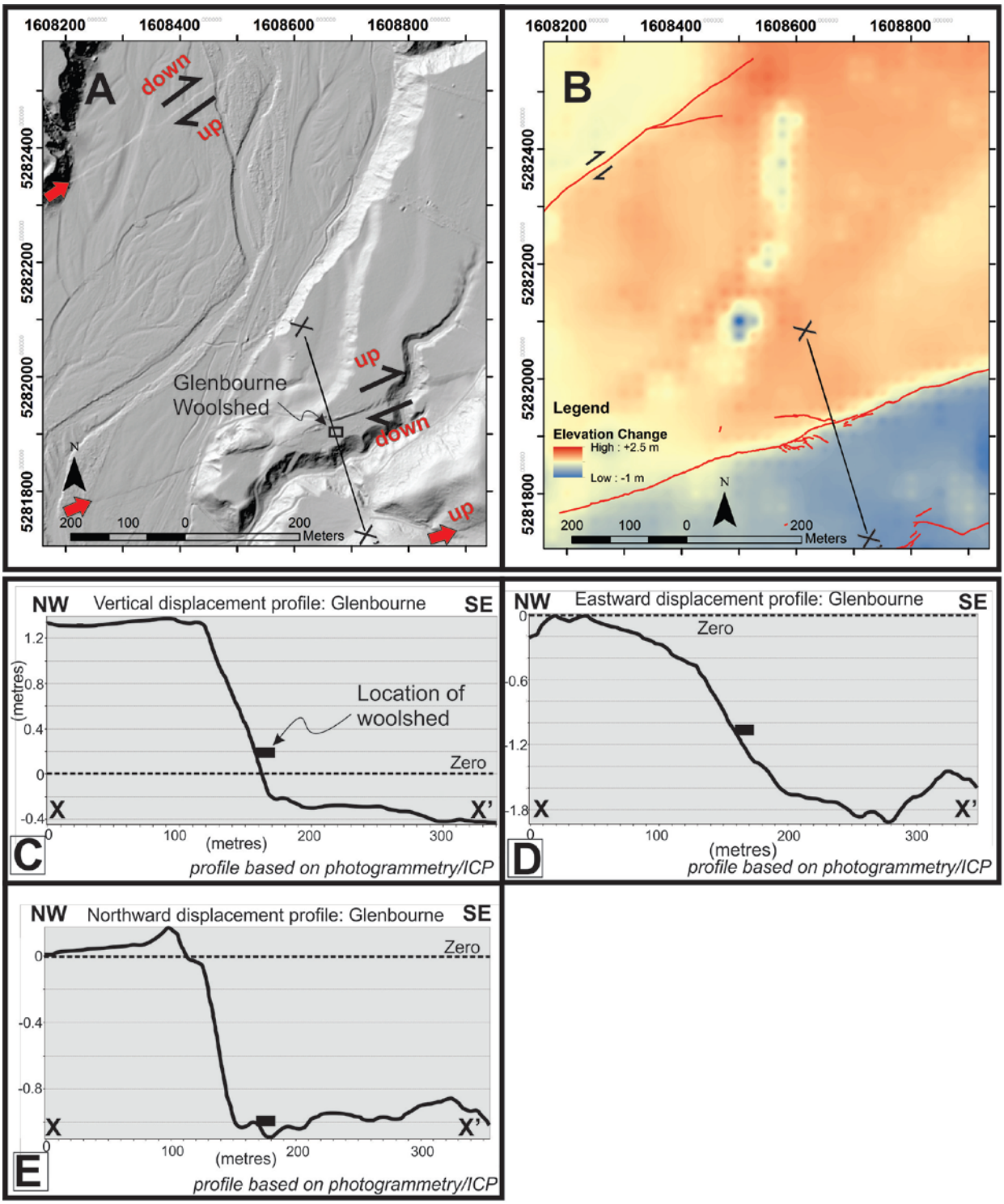

Figure 14: Glenbourne Woolshed and surface rupture of The Humps Fault. (A) LiDAR hill shade DEM showing location of the woolshed and two prominent discrete fault traces (red arrows), one of which is within ~5 m of the woolshed (see Figures 13A & 13C). (B) Raster of vertical displacements in the same area as (A), using ICP method outlined in the text. (C), (D), and (E) are the vertical, eastward, and northward displacement profiles from X to X' on the top two images. The location of the woolshed is shown on each profile. Note that while relative motions were mapped in the field, the absolute sense of displacement is more complex, with the downthrown side of the fault moving southwestward and the up-thrown side of the fault remaining relatively stable except in the vertical direction. Y-axis exaggeration in (C) & (D) = 85. Y-axis exaggeration in (E) = 130.

depression that transitions to the east into a narrow zone of Riedel shears and tension fractures (Figures 15 & 16A). In the field, an adjacent fault-offset fence yielded RTK-derived offset measurements of 0.9 m dextral and 0.5 m vertical [4]. The cottage experienced a chimney collapse (Figure 15B), and multiple fractures to the concrete foundation (Figures 15C & 15D). Timber supports for the roof/veranda at the front the cottage experienced minor amounts of shear, and were deformed out-of-plumb (Figures 15C & 15D). Several cladding planks at the base of the exterior of the cottage were broken (Figure 15D). Although surface rupture caused structural damage to the cottage, the cottage appears to be far from collapse. Using a combination of the ICP-based analysis (see

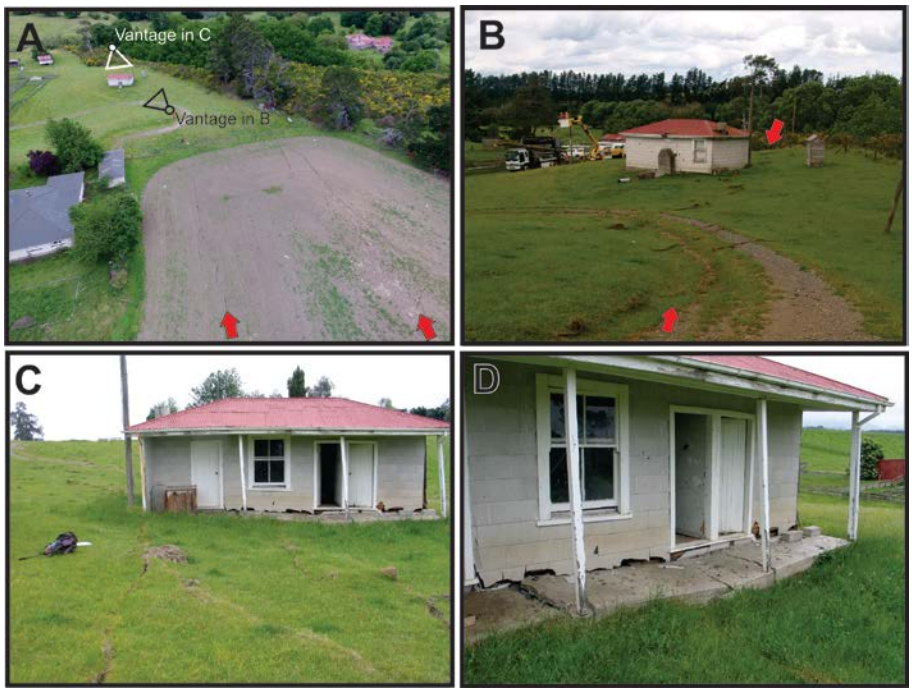

Figure 15: Hillview Cottage and surface rupture of The Humps Fault; see Figures 1 & 16 for location (Lat: -42.6287, Long: 173.0154). (A) Oblique aerial view looking east towards the cottage, along discrete dextral-normal surface fault ruptures (red arrows). Photo courtesy of Sam McColl taken from a drone in November 2016. (B) View looking northeast. At this location, the cottage is impacted by decimetre-scale discrete fault rupture (in this case Riedel shears) and centimetres to decimetres of distributed deformation between the shears. Note the collapsed chimney. Photo taken by Clark Fenton in November 2016. (C) & (D) Details of damage to the cottage caused by decimetre-scale surface fault rupture. Photos taken by Jarg Pettinga in November 2016.

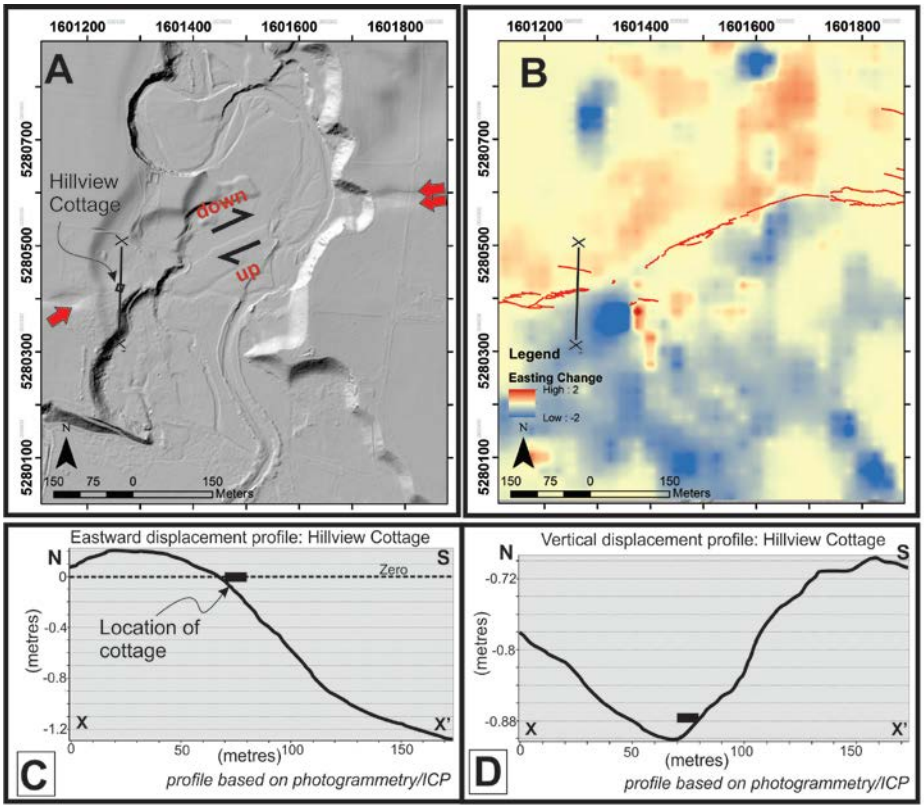

Figure 16: Hillview Cottage and The Humps Fault surface rupture. (A) LiDAR hill shade DEM showing location of the cottage within a relatively narrow fault rupture deformation zone (red arrows). (B) Raster of displacement in the east direction (positive is east, negative is west) calculated using ICP method described in text. Some anomalies and artefacts of the grid exist within the dataset but the overall pattern is one of predominantly dextral displacement. West of the cottage is a small pull-apart, while the 100 m-scale fault geometry is that of a restraining bend. (C) & (D) The eastward and vertical deformation profiles from X to X', respectively. Y-axis exaggeration in (C) = 60. Y-axis exaggeration in (D) = 385.

Glenbourne section), and field observations, we estimate centimetre-scale vertical and decimetre-scale dextral displacement at the site of the cottage. Assuming simple shear and a sub-vertical fault plane, we estimate a net shear strain across the foot print of the structure of ~10^{-2}.

Mendip Deer Shed – The Leader Fault

The Mendip deer shed is a single-storey steel-framed structure with corrugated metal roof and cladding. Light steel trusses are mounted on light steel columns, emplaced in concrete footings, with wire bracing elements in walls and roof. The exterior walls incorporate timber-framing and internal separators between crush, race, and pens are a mix of light steel and ply-clad partitions mounted on poles, and pole-mounted timber planks. It has a rectangular floor plan of ~235 m^2. The floor is concrete that was poured on grade and is not structural.

Mendip deer shed was constructed in 2004, and is sited on a thin veneer of late Quaternary fluvial gravel (<2 m) overlying weak to moderately strong bedrock.

Mendip Station is located along the Mt. Stewart rangefront and the northern Leader Fault (Figures 1, 17 & 18) [4]. At the general location of the deer shed, the surface rupture of the Leader Fault swings in strike by about 90°; the general strike of the rupture to the west is east-west, and to the east it is north-south (Figure 18). Along this portion of rupture, the predominant sense of displacement is reverse (northwest-side up). Field-measured displacements indicate ~1 m of throw and decimetre to metre-scale sinistral and dextral strike-slip displacements west and north of the bend, respectively. At the deer shed location, northwest trending reverse and normal faults intersect the frontal thrust and accommodate some of the opposite-sense strike slip (Figure 18). Traces of these secondary

Figure 17: Mendip deer shed and northern Leader Fault surface rupture; see Figures 1 & 18 for location (Lat: -42.5740, Long: 173.2825). (A), (B), & (C) Field photographs of normal faulting running through the deer shed. (B) is looking to the southeast, across the stock yard and towards the intersection of the two fault sets (see text for discussion). Photos taken by Clark Fenton in January 2017.

faults were tracked through the deer shed floor and into the adjacent stock yards (Figure 17).

Damage to the deer shed was relatively minor and limited to some cracking of the concrete floor, and separation of the walls from the floor (Figure 17). Most of the damage is linked to the relatively minor, discrete displacements on the northwest trending secondary faults, as distributed deformation from the main thrust (~25 m to the southeast) is limited. This does, however, highlight the fact that complex fault kinematics can result in secondary faulting that can directly impact engineered structures. These secondary features may not be evident in the landscape over geologic timescales due their relatively small scale and commensurate poor preservation potential, but might be anticipated with detailed mapping and documentation of the primary fault trace geometry and kinematics. Shear strain estimates are complicated by the intersecting set of faults at this location, but we estimate strains on the order of 10^{-1} – 10^{-2}.

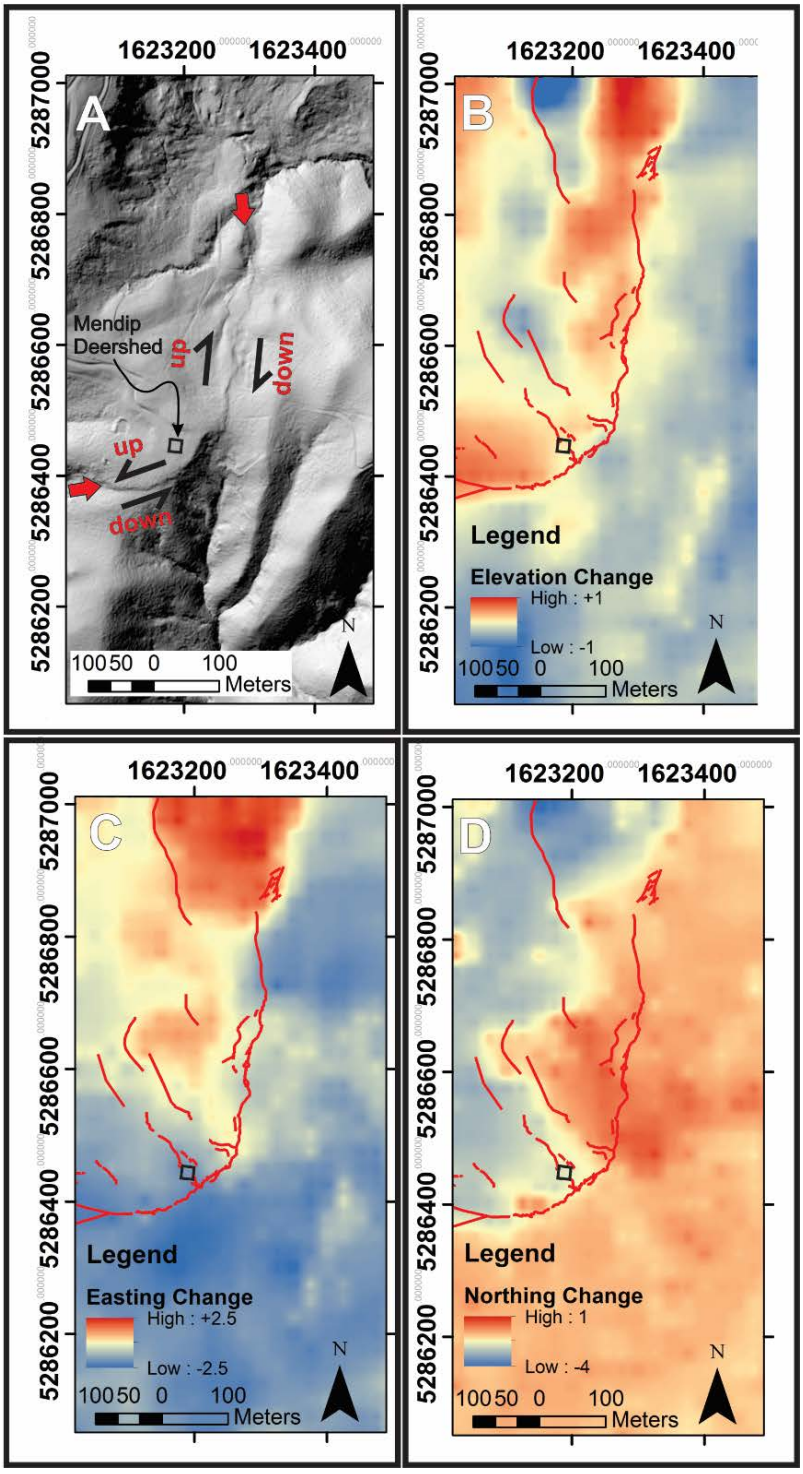

Figure 18: The Mendip deer shed and surface rupture along the northern Leader Fault. (A) LiDAR hill shade with location of the deer shed indicated. The primary fault trace (red arrows) and sense of slip are indicated. (B) The fault traces with elevation change raster determined using ICP method described in text. (C) Same as (B), but for easting change (positive values moved east). (D) Same as in (B), but for northing change (positive values moved north). Note that compression and associated reverse faulting predominates, with components of sinistral and dextral sense west and north of the deer shed, respectively. However, discrete faulting on secondary NW-SE striking faults was the main contributor to deer shed damage.

DISCUSSION

In a large earthquake, surface fault rupture deformation places additional demands on structures, compared to similar structures exposed only to strong ground shaking. Based on the building damage examples presented in this paper (e.g. Figures 2, 3 5-18) for the 2016 Kaikōura earthquake, and those presented by Van Dissen et al. [21] for the 2010 Darfield earthquake, some pertinent observations can be made regarding the performance of New Zealand residential structures when subjected to surface fault rupture deformation of varying levels of strain and amounts of displacement.

1. Single-storey, regular-shaped, timber-framed residential structures with light roofs and of modest dimensions (floor area of ≤~200 m^2) subjected to low/moderate surface fault rupture deformation (i.e., shear strains ≤10^{-2} and discrete displacements of decimetre-scale or less) do not appear to pose a collapse hazard.
2. At those levels of deformation, the prospects of damage-control and repairability (and therefore post-event functionality) appear to be improved for such residential structures if the cladding contributes to the robustness to the superstructure (e.g., plywood, timber weather board), and is not brittle.
3. This favourable behaviour is enhanced if building systems moderate the direct transmission of ground deformation into the superstructure (either by decoupling or by other means), and allow for re-levelling of the structure post-event. For additional discussion regarding the mitigation of surface fault rupture hazed via the decoupling of ground deformation from the superstructure see, for example, Lazarte et al. [24], Murbach et al. [25], Bray [26, 27], Bray and Kelson [28], Van Dissen et al. [21], and Oettle and Bray [29].
4. For residential structures with the above-mentioned attributes, non-collapse performance can be achieved at even higher levels of strain (~10^0) and larger discrete displacements (metre-scale) in a predominantly horizontal displacement setting (i.e., strike slip) if the superstructure decouples from (is isolated from) the underlying ground deformation. Our New Zealand dataset does not contain examples of the performance of residential structures subjected to such large surface fault rupture strains and displacements in a predominantly vertical displacement setting. In a horizontal displacement setting the decoupled superstructure still rests on (and is supported by) the ground (e.g. Figure 3). This may not be the case in a predominantly vertical displacement setting where there is the possibility that fault rupture will leave a significant portion of the decoupled superstructure un-supported and this may lead, if not to collapse, then at least to significant tilting and angular distortions. In addition, in a reverse/thrust vertical displacement setting there is the potential for a "bulldozer zone" to develop at the base of the scarp where fault displacement forces the scarp to thrust horizontally across the ground surface, and this too can severely impact structures [20].

In New Zealand, the primary document providing guidance with regards to the mitigation of surface fault rupture hazard is the Ministry for the Environment (MfE) report titled "Planning for development of land on or close to active faults: a guideline to assist resource management planners in New Zealand" [30, see also 31]. In this guidance document, with its life-safety focus, a distinction is made between single-storey timber-framed residential structures (Building Importance Category 2a structures – i.e., BIC 2a structures) and other normal structures (BIC 2b structures) with more permissive resource consent categories applied to the former. The non-collapse performance of single-storey timber-framed structures when subjected to surface fault rupture in the 2016 Kaikōura earthquake (and also in the 2010 Darfield earthquake [21]) strongly supports this distinction. In addition, the MfE document makes a distinction between *well-defined* (i.e., concentrated) deformation and *distributed* deformation with more restrictive resource consent categories applied to the former. Our observations that the severity of damage, in general, increases with both increasing total displacement and increasing strain supports this distinction.

The MfE guidance document also recommends that the siting and construction of a BIC 2a structure (i.e., single-storey timber-framed house) in a greenfield setting within a distributed deformation zone of an active fault with a recurrence interval ≤3500 years be considered a *Discretionary* activity. However, given the life-safety focus of the MfE guidance document, and the non-collapse performance of BIC 2a structures – especially when subjected to distributed lower strain surface fault rupture deformation – consideration could be given to adopting a more permissive resource consent category such as *Controlled*. Nevertheless, we must stress that consideration of more permissive resource consent categories is only germane from a life-safety perspective. From a damage-control perspective, or a post-event-functionality perspective, application of more permissive resource consent categories will, in general, run counter to those objectives.

CONCLUSIONS

About a dozen buildings, typically single-storey timber-framed houses, barns and wool sheds with regular shaped floor plans and lightweight roofing materials were directly impacted by surface fault rupture in the 2016 Kaikōura earthquake. The amount and style of surface rupture deformation varied considerably, ranging from decimetre-scale distributed folding with estimated shear strains in the order of ≤10^{-2}, to metre-scale discrete rupture with estimated shear strains up to 10^0. While the severity of damage generally increased with both increasing total displacement and increasing strain none of these buildings collapsed. From a life-safety standpoint, all these buildings performed well and provide insight into construction styles that could best be employed to facilitate non-collapse performance resulting from surface fault rupture and, in certain instances, post-event functionality.

ACKNOWLEDGEMENTS

We gratefully acknowledge and thank the many landowners for allowing access to their properties during trying times. Funding was provided by GeoNet (with the support of its sponsors EQC, GNS Science, LINZ), MBIE response funding (provided through NHRP grant 2017-GNS-01-NHRP), and GNS Science (provided through MBIE strategic science investment funding). UC staff acknowledge the financial support received from the University of Canterbury and EQC. NSF-GEER funding supported T. Stahl. We thank two anonymous reviewers for their constructive, and improving, comments.

REFERENCES

1 Downes GL and Dowrick DJ (2014). "*Atlas of Isoseismal Maps of New Zealand Earthquakes - 1843-2003*". Second edition (revised). GNS Science monograph 25. ISBN 978-0-478-196634. 797 pp.

2 GNS Science (2018). *GeoNet*. https://www.geonet.org.nz/earthquake/story. (Accessed 25/5/2018).

3 Litchfield NJ, Villamor P, Van Dissen RJ, Nicol A, Barnes PM, Barrell DJA, Pettinga J, Langridge RM, Little TA, Mountjoy J, Ries W, Rowland J, Fenton C, Stirling MW, Kearse J, Berryman K, Cochran UA, Clark KJ, Hemphill-Haley M, Khajavi N, Jones K, Archibald G, Upton P, Asher C, Benson A, Cox SC, Gasston C, Hale D, Hall B, Hatem A, Heron DW, Howarth J, Kane T, Lamarche G, Lawson S,

Lukovic B, McColl S, Madugo C, Manousakis J, Noble D, Pedley K, Sauer K, Stahl T, Strong DT, Townsend DB, Toy V, Williams J, Woelz S and Zinke R (2018). "Surface rupture of multiple crustal faults in the 2016 M_w 7.8 Kaikōura, New Zealand, earthquake". *Bulletin of the Seismological Society of America*, **108**(3B): 1496–1520. doi: 10.1785/ 0120170300.

4 Nicol A, Khajavi N, Pettinga J, Fenton C, Stahl T, Bannister S, Pedley K, Hyland-Brook N, Bushell T, Hamling I, Ristau J, Noble D and McColl ST (2018). "Preliminary geometry, displacement, and kinematics of fault ruptures in the epicentral region of the 2016 M_w 7.8 Kaikōura, New Zealand, earthquake". *Bulletin of the Seismological Society of America*, **108**: 1521-1539. doi: 10.1785/0120170329.

5 Holden C, Kaiser A, Van Dissen R and Jury R (2013). "Sources, ground motion, and structural response characteristics in Wellington of the 2013 Cook Strait earthquakes". *Bulletin of the New Zealand Society for Earthquake Engineering*, **46**(4): 188-195.

6 Langridge RM, Ries WF, Litchfield NJ, Villamor P, Van Dissen RJ, Rattenbury MS, Barrell DJA, Heron DW, Haubrock S, Townsend DB, Cox SC, Berryman KR, Nicol A, Lee JM and Stirling MW (2016). "The New Zealand Active Faults Database". *New Zealand Journal of Geology and Geophysics*, **59**(1): 86–96.

7 Bradley BA, Razafindrakoto HNT and Nazer MA (2017). "Strong ground motion observations of engineering interest from the 14 November 2016 M_w 7.8 Kaikōura, New Zealand earthquake". *Bulletin of the New Zealand Society for Earthquake Engineering*, **50**(2): 85-83.

8 Kaiser A, Balfour N, Fry B, Holden C, Litchfield N, Gerstenberger M, D'Anastasio E, Horspool N, McVerry G, Ristau J, Bannister S, Christophersen A, Clark K, Power W, Rhoades D, Massey C, Hamling I, Wallace L, Mountjoy J, Kaneko Y, Benites R, Van Houtte C, Dellow S, Wotherspoon L, Elwood K and Gledhill K (2017). "The Kaikōura (New Zealand) Earthquake: Preliminary seismological report". *Seismological Research Letters*, **88**(3): 727-739.

9 Dellow S, Massey C, Cox S, Archibald G, Begg J, Bruce Z, Carey J, Davidson J, Della Pasqua F, Glassey P, Hill M, Jones K, Lyndsell B, Lukovic B, McColl S, Rattenbury M, Read S, Rosser B, Singeisen C, Townsend D, Villamor P, Villeneuve M, Godt J, Jibson R, Allstadt K, Rengers F, Wartman J, Rathje E, Sitar N, Adda A-Z, Manousakis J and Little M (2017). "Landslides caused by the M_w 7.8 Kaikōura Earthquake and the immediate response". *Bulletin of the New Zealand Society for Earthquake Engineering*, **50**(2): 106-116.

10 Massey C, Townsend D, Rathje E, Allstadt K, Kaneko Y, Lukovic B, Bradley B, Wartman J, Horspool N, Hamling I, Carey J, Cox S, Davidson J, Dellow S, Holden C, Jibson R, Jones K, Kaiser A, Little M, Lyndsell B, McColl S, Morgenstern R, Petley DN, Rengers F, Rhoades D, Rosser B, Strong D, Singeisen C and Villeneuve M (2018). "Landslides triggered by the M_w 7.8 14 November 2016 Kaikōura earthquake, New Zealand". *Bulletin of the Seismological Society of America*, **108**(3B): 1630-1648. doi: 10.1785/ 0120170305.

11 Cubrinovski M, Bray JD, De La Torre C, Olsen MJ, Bradley BA, Chiaro G, Stocks E and Wotherspoon L (2017). "Liquefaction effects and associated damages observed at the Wellington Centreport from the 2016 Kaikōura earthquake". *Bulletin of the New Zealand Society for Earthquake Engineering*, **50**(2): 152-173.

12 Stringer ME, Bastin S, McGann CR, Cappellaro C, El Kortbawi M, McMahon R, Wotherspoon LM, Green RA, Aricheta J, Davis R, McGlynn L, Hargraves S, Van Ballegooy S, Cubrinovski M, Bradley BA, Bellagamba X, Foster K, Lai C, Ashfield D, Baki A, Zekkos A, Lee R and Ntritsos N (2017). "Geotechnical aspects of the 2016 Kaikōura earthquake on the South Island of New Zealand". *Bulletin of the New Zealand Society for Earthquake Engineering*, **50**(2): 117-141.

13 Bastin SH, Ogden M, Wotherspoon LM, van Ballegooy S, Green RA and Stringer M (2018). "Geomorphological influences on the distribution of liquefaction in the Wairau Plains, New Zealand, following the 2016 Kaikōura earthquake". *Bulletin of the Seismological Society of America*, **108**(3B): 1683-1694. doi: 10.1785/0120170248.

14 Clark K, Nissen E, Howarth J, Hamling I, Mountjoy J, Ries W, Jones K, Goldstein, S, Cochran U, Villamor P, Hreinsdóttir S, Litchfield N, Berryman K and Strong D (2017). "Highly variable coastal deformation in the 2016 M_w 7.8 Kaikōura earthquake reflects rupture complexity along a transpressional plate boundary". *Earth and Planetary Science Letters*, **474**: 334-344.

15 Power W, Clark K, King D, Borrero J, Howarth J, Lane E, Goring D, Goff J, Chague-Goff C, Williams J, Reid C, Whittaker C, Mueller C, Williams S, Hughes M, Hoyle J, Bind J, Strong D, Litchfield N and Benson A (2017). "Tsunami runup and tide-gauge observations from the 14 November 2016 M7.8 Kaikōura earthquake, New Zealand". *Pure and Applied Geophysics*, **174**: 2457-2473.

16 Hamling IJ, Hreinsdóttir S, Clark K, Elliott J, Liang C, Fielding E, Litchfield N, Villamor P, Wallace L, Wright TJ, D'Anastasio E, Bannister S, Burbidge D, Denys P, Gentle P, Howarth J, Mueller C, Palmer N, Pearson C, Power W, Barnes P, Barrell D, Van Dissen R, Langridge R, Little T, Nicol A, Pettinga J, Rowland J and Stirling M (2017). "Complex multi-fault rupture during the 2016 M_w 7.8 Kaikōura earthquake, New Zealand". *Science*, **356** (6334), eaam7194. doi: 10.1126/science.aam7194.

17 Stirling MW, Litchfield NJ, Villamor P, Van Dissen RJ, Nicol, A, Pettinga J, Barnes P, Langridge RM, Little T, Barrell DJA, Mountjoy J, Ries WF, Rowland J, Fenton C, Hamling I, Asher C, Barrier A, Benson A, Bischoff A, Borella J, Carne R, Cochran UA, Cockroft M, Cox SC, Duke G, Fenton F, Gasston C, Grimshaw C, Hale D, Hall B, Hao KX, Hatem A, Hemphill-Haley M, Heron DW, Howarth J, Juniper Z, Kane T, Kearse J, Khajavi N, Lamarche G, Lawson S, Lukovic B, Madugo C, Manousakis I, McColl S, Noble D, Pedley K, Sauer K, Stahl T, Strong DT, Townsend DB, Toy V, Villeneuve M, Wandres A, Williams J, Woelz S and Zinke R (2017). "The M_w 7.8 Kaikōura earthquake: Surface rupture, and seismic hazard context". *Bulletin of the New Zealand Society for Earthquake Engineering*, **50**(2): 73-84.

18 Kearse J, Little TA, Van Dissen RJ, Barnes PM, Langridge R, Mountjoy J, Reis W, Villamor P, Clark KJ, Benson A, Lamarche G, Hill M and Hemphill-Haley M (2018). "Onshore to offshore ground-surface and seabed rupture of the Jordan-Kekerengu-Needles fault network during the 2016, M_w 7.8 Kaikōura earthquake, New Zealand". *Bulletin of the Seismological Society of America*, **108**(3B): 1573–1595. doi: 10.1785/0120170304.

19 Langridge RM, Rowland J, Villamor P, Mountjoy J, Townsend DB, Nissen E, Madugo C, Ries WF, Gasston C, Canva A, Hatem AE and Hamling I (2018). "Coseismic rupture and preliminary slip estimates for the Papatea fault and its role in the 2016 M_w 7.8 Kaikōura, New Zealand, earthquake". *Bulletin of the Seismological Society of America*, **108**(3B): 1596-1622. doi: 10.1785/0120170336.

20 Kelson KI, Kang K-H, Page WD, Lee C-T and Cluff LS (2001). "Representative styles of deformation along the Chelungpu fault from the 1999 Chi-Chi (Taiwan) Earthquake: geomorphic characteristics and responses of

man-made structures". *Bulletin of the Seismological Society of America*, **91**: 930-952.

21 Van Dissen R, Barrell D, Litchfield N, Villamor P, Quigley M, King A, Furlong K, Begg J, Townsend D, Mackenzie H, ahl T, Noble D, Duffy B, Bilderback E, Claridge J, Klahn A, Jongens R, Cox S, Langridge R, Ries W, Dhakal R, Smith A, Hornblow S, Nicol R, Pedley K, Henham H, Hunter R, Zajac A and Mote T (2011). "Surface rupture displacement on the Greendale Fault during the M_w 7.1 Darfield (Canterbury) earthquake, New Zealand, and its impact on man-made structures". *Proceedings of the 9th Pacific Conference on Earthquake Engineering*, Auckland, New Zealand, 14-16 April 2011, Paper No 186, 8 pp.

22 Nissen E, Krishnan AK, Arrowsmith JR and Saripalli S (2012). "Three-dimensional surface displacements and rotations from differencing pre- and post-earthquake LiDAR point clouds". *Geophysical Research Letters*, **39**, doi: 0.1029/2012GL052460.

23 Davies AJ, Sadashiva V, Aghababaei M, Barnhill D, Costello SB, Fanslow B, Headifen D, Hughes M, Kotze R, Mackie J, Ranjitkar P, Thompson J, Troitino DR, Wilson T, Woods S and Wotherspoon LM (2017). "Transportation infrastructure performance and management in the South Island of New Zealand, during the first 100 days following the 2016 M_w 7.8 "Kaikōura" earthquake". *Bulletin of the New Zealand Society for Earthquake Engineering*, **50**(2): 271-299.

24 Lazarte CA, Bray JD, Johnson AM and Lemmer RE (1994). "Surface breakage of the 1992 Landers earthquake and its effect on structures". *Bulletin of the Seismological Society of America*, **84**: 547-561.

25 Murbach D, Rockwell TK and Bray JD (1999). "The relationship of foundation deformation to surface and near-surface faulting resulting from the 1992 Landers earthquake". *Earthquake Spectra*, **15**: 121-144.

26 Bray JD (2001). "Developing mitigation measures for the hazards associated with earthquake surface fault rupture". *Proceedings of the Workshop on Seismic Fault-Induced Failures*, Tokyo, Japan, 11-12 January 2001: 55-79.

27 Bray JD (2009). "Designing buildings to accommodate earthquake surface fault rupture". *Proceedings 2009 ATC and SEI Conference on Improving the Seismic Performance of Existing Buildings and Other Structures*, San Francisco, USA, 9-11 December 2009: 1269-1280.

28 Bray JD and Kelson KI (2006). "Observations of surface fault rupture from the 1906 earthquake in the context of current practice". *Earthquake Spectra*, **22**(S2): S69-S89.

29 Oettle NK and Bray JD (2013). "Geotechnical mitigation strategies for earthquake surface fault rupture". *Journal of Geotechnical and Geoenvironmental Engineering*, **139**(11): 1864-1974.

30 Kerr J, Nathan S, Van Dissen R, Webb P, Brunsdon D and King A (2003). "*Planning for development of land on or close to active faults: A guideline to assist resource management planners in New Zealand*". Ministry for the Environment ME number 483, 67 pp. (http://www.mfe.govt.nz/sites/default/files/media/RMA/planning-development-faults-graphics-dec04%20%281%29.pdf)

31 Van Dissen R, Heron D, Kerr J, Guerin A, Muspratt M and Hinton S (2006). "Mitigating active fault surface rupture hazard in New Zealand: development of national guidelines, and assessment of their implementation". *Proceedings of the 8th U.S. National Conference on Earthquake Engineering*, San Francisco, California, 18-22 April 2006, Paper No 633, 10 pp.